

CONCEPT OF VISCOUS HEATING TO REINVENT
THE TOILET

By

MD.WALIUL ISLAM

Bachelor of Science in Chemical Engineering

Bangladesh University of Engineering & Technology

Dhaka, Bangladesh

2008

Submitted to the Faculty of the
Graduate College of the
Oklahoma State University
in partial fulfillment of
the requirements for
the Degree of
MASTER OF SCIENCE
December, 2013

CONCEPT OF VISCOUS HEATING TO REINVENT
THE TOILET

Thesis Approved:

Gary L. Foutch

Thesis Adviser

A. H. Johannes

James E. Smay

Heather Fahlenkamp

ACKNOWLEDGEMENTS

It started with a great discussion with my thesis advisor Dr. Gary L. Foutch in September of 2011. I was looking for my master thesis advisor and he was looking for a graduate to work in his “Reinvent the Toilet” project funded by Bill and Melinda Gates Foundation. At the very first meeting he gave me piece information, “Toilet is the most important discovery in last two hundred years which saved more lives than any other discovery.” That day I decided to work with something different than traditional. I am grateful to this person for his effective mentorship and a flexible mentality to help me grow a better human being. Also I worked with Dr. AJ Johannes and experience how liberal people of this country are to accept new ideas. Jagdeep T. Podichetty, one of my colleagues, currently doing his PhD in the same program helped me improve the Computational Fluid Dynamics part. Jagdeep’s strong desire to establish things always pushed me to finish work on time. I was taught the rheology experiment by Kunpeng Cai and Yang Shi from Dr. Smay’s Laboratory. I would like to thank Mr. Ronny E Markum of the Advanced Technology Research Center, Oklahoma State University for assisting with the design, building the equipment and troubleshoot the operation. I owe to Ms. Shelley Potter, the Lab Manager for welcoming attitude to help. All these great people, you can meet if you visit Oklahoma State University, Stillwater, Oklahoma.

Md. Waliul Islam

December, 2013

Name: MD.WALIUL ISLAM

Date of Degree: DECEMBER, 2013

Title of Study: CONCEPT OF VISCOUS HEATING TO REINVENT THE TOILET

Major Field: CHEMICAL ENGINEERING

Abstract: Highly viscous substances, such as feces, produce significant heat when layer deformation occurs. We describe the use of viscous heating to destroy disease-causing microorganisms and whipworms in feces using little power. The laboratory-scale unit has a rotating central core with a space between a fixed shell wall. Viscous heating of feces proved effective for disinfection. Data were obtained over a range of operating conditions with simulant materials. In addition, baboon feces were tested for parasite destruction. For simulants, the temperature observed with the smallest spacing approached 200°C. Baboon feces showed 99% destruction of *Trichuris trichiura* as a result of shear stress only because temperature was limited as a result of heat in samples. Vegetable dye through the reactor demonstrated plug flow. Alternative geometries are considered for high-volume sludge processing. Design modifications include enhancing efficient water evaporation and recovery. Since the process can sterilize fecal mass, other treatment technologies should consider integrating viscous heating into their process streams.

TABLE OF CONTENTS

Chapter	Page
I. INTRODUCTION.....	1
1.1 Background.....	2
1.2 Our Proposal	4
II. COMPUTATIONAL FLUID DYANAMICS	8
2.2 Governing Equations	8
2.3 Analysis of Geometry	10
III. RHEOLOGY AND OTHER PROPERTIES	12
3.1 Experimental Method.....	12
3.2 Fake Stool Preparation.....	17
3.3 Moisture Content of Potato.....	19
3.4 Density of Potato.....	20
IV. EXPERIMENTATION WITH SIMULANT	23
4.1 Feed Preparation	23
4.2 Operating Technique.....	24
V. RESULTS AND DISCUSSION	29
5.1 Temperature Gradient Obtained from CFD	29
5.1.1 Effect of Dimension.....	29
5.1.2 Effect of Inlet Velocity	31
5.1.3 Effect of Angular Velocity.....	32
5.2 Heat Generation in Simulant (Red Potato)	32
5.3 Results of Longer Operation.....	36
5.4 Parasite Destruction	39
5.5 Experiment with Additives.....	41

5.6 Peanut Butter Experiment	42
5.7 Reactor Profile	43
5.8 Shear Stress Analysis	47
5.8.1 Comparison of Inlet and Outlet Tangential Shear Rate	48
5.8.2 Comparison of Inlet and Outlet Axial Shear Rate	49
5.9 Volume of the Reactor	49
5.10 Second Prototype	49
VI. ENERGY BALANCE	53
6.1 Work Done by the Plunger	54
6.2 Work Done by the Motor	55
6.3 Kinetic Energy of the Shaft.....	56
6.3.1 Moment of Inertia of Cone	57
6.3.2 Moment of Inertia of Connecting Cylinder	59
6.3.3 Moment of Inertia of Lovejoy Coupling Joint.....	60
6.4 Heat Gain by the Product.....	61
6.5 Final Energy Balance & System Efficiency	62
VII. CONCLUSION	64
7.1 Challenges.....	65
7.2 Fecal Sludge Business.....	66
REFERENCES	69
APPENDICES	74
Appendix A Installation of the Shear Reactor	74
Appendix B Operating Manual of the Shear Reactor	80
Appendix C Model Development	88
Appendix D Frequency vs. RPM Plot.....	104
Appendix E Rotating Parts & Accessories	105

LIST OF TABLES

Table	Page
1 Assumption of Fluid Properties to Simulate in CFD	11
2 Composition of Fake Stool	17
3 Moisture Content in Boiled Pieced Potato after 6 hours of Drying at 35° C.....	19
4 Moisture Content in Boiled Mashed Potato after 22 hour of Drying at 45°C	20
5 Density Determination of Red Potato before Boiling.....	21
6 Density Determination of Red Potato after Boiling.....	22
7 Temperature Rise with Time at Constant Feed Pressure, RPM and Spacing	33
8 Temperature Rise with Spacing Change at Constant Pressure, RPM and Time ...	33
9 Temperature Rise with RPM change at Constant Pressure, Time and Spacing	34
10 Temperature with Time at 70 psig, 0.75 mm spacing and 1790 RPM	35
11 Percentage Parasite Egg Destruction with Variable Settings	39
12 Experimental Result for Peanut Butter Run.....	43
13 Outlet Temperature Reading for Different Holdup Time	52
14 Outlet Temperature for Different Holdup Time at 0.75mm Spacing, 1210 RPM and 100 psig Feed Pressure	88
15 Outlet Temperature for Different Hold up Time at 1mm Spacing, 1210 RPM and 100 psig Feed Pressure	89
16 Outlet Temperature for Different Holdup Time at 1.25 mm Spacing, 1210 RPM and 100 psig Feed Pressure	90
17 Outlet Temperature for Different Hold up Time at 0.75 mm Spacing, 1800 RPM and 100 psig Feed Pressure	91
18 Outlet Temperature for Different Hold up Time at 0.75mm Spacing, 1505 RPM and 100 psig Feed Pressure	92
19 Outlet Temperature for Hold up Tie at 0.75 mm, 1210 RPM and 100 psig Feed Pressure 100 psig Feed Pressure	93
20 Outlet Temperature for Different Hold up Time at 0.75mm Spacing, 912 RPM and 100 psig Feed Pressure	94
21 Outlet Temperature for Different RPM at 0.75mm Spacing, 180 seconds Holdup Time and 100 psig Feed Pressure.....	95
22 Outlet Temperature for Different RPM ant 0.75 mm Spacing, 120 Seconds Holdup Time and 100 psig Feed Pressure.....	96
23 Outlet Temperature for Different RPM ant 0.75mm Spacing, 60 seconds Holdup Time and 100 psig Feed Pressure.....	97
24 Outlet Temperature for Different Spacing at 180 seconds Holdup Time, 1210 RPM and 100 psig Feed Pressure.....	98

25	Outlet Temperature for Different Spacing at 120 seconds Holdup Time, 1210 RPM and 100 psig Feed Pressure	99
26	Outlet Temperature for Different Spacing at 60 seconds Holdup Time, 1210 RPM and 100 psig Feed Pressure	100
27	$\frac{\partial \theta}{\partial t}$ Values with Different RPM at 0.75mm Spacing.....	102
28	$\frac{\partial \theta}{\partial t}$ Values with Different Spacing at 1210 RPM.....	102
29	$\frac{\partial \theta}{\partial r}$ Values with Different Holdup Time at 0.75 mm Spacing.....	103
30	$\frac{\partial \theta}{\partial s}$ Values with Different Holdup Time at 1210 RPM	103
31	Hz (inverter reading) and Tachometer Reading without any Load Outlet	104

LIST OF FIGURES

Figure	Page
1 Design Model Setup and Boundary Conditions.....	9
2 Reactor Geometry Used for CFD Studies.....	11
3 CVOR Bohlin Rheometer.....	12
4 Plastic Cup (left) and Balls (right) for Grinding Feed	13
5 Thinky Grinding Machine.....	13
6 Serrated Cylinder (Left) and Rotating Shaft (Right)	14
7 Black Rubber (Left) and Plastic Semi-Circular Plate with Filter Paper (Right)....	15
8 Final Setup for Viscosity Measurement.....	15
9 Poly Science Water Circulating Heating System.....	16
10 Computer Demonstration for Viscosity Data Gathering	16
11 Fake Stool Preparation.....	18
12 Shear Rate Decrease with Viscosity for Various Feces and Simulants	19
13 Digital Weighing Scale from Fisher Scientific	21
14 Mashing Potatoes with Masher.....	24
15 Making Smooth Paste with Ricer	24
16 Instrumentation on Reactor to Process Fecal Sludge and Simulant Solids	25
17 The Cone (left) Rotates inside the Housing (right).....	26
18 A Typical Setup of the Cone inside the Housing with Spacing Controller and Outlet Cork (Black).....	27
19 Effect of Length with Semi-Angle = 21.8° and Clearance = 0.001m.....	29
20 Effect of Semi-Angle with Length = 1 m and Clearance = 0.001 m	30
21 Effect of Clearance with Length = 0.1 m and Semi-Angle = 21.8°	31
22 Temperature Gradient with Inlet Velocity 0.002 m/s at 500 rpm.....	31
23 Temperature with Time at 100 psig, 1800 RPM and 0.75 mm Spacing.....	33
24 Temperature with Spacing at 100 psig, 1210 RPM and 180 seconds Time	34
25 Temperature with RPM at 100 psig, 180 seconds Time and 0.75 mm Spacing ..	36
26 Burnt Mashed Potato Layer over the Cone Surface.....	37
27 The Cone and the Shell after 8 minutes (480 seconds) Run	38
28 Photomicrographs of <i>Trichuris trichiura</i> Eggs from Helium before Being Processed through the Extruder (400 x Magnifications).....	39
29 Photomicrographs of <i>Trichuris trichiura</i> Eggs from Helium after Being Processed through the Extruder (400 x Magnifications).....	40
30 Temperature Reading for Experimentation with Grass, Sweet Potato & Toilet Paper	41
31 Product of Experimentation with Grass, Toilet Paper & Sweet Potato	42

32 Charging Mashed Potatoes Manually by Operator	44
33 Vegetable Dye Passing through the Reactor to Determine Flow Pattern	44
34 Dimension of the Cone and Other Rotating Parts.....	45
35 Shear Rate Analysis	47
36 Determination of Volume inside the Reactor	50
37 Water Leak from the Reactor when Charged	50
38 Design Improvement of the Viscous Heating Mechanism (Second Unit).....	51
39 Power versus Time for no Load and Load Conditions at 100 psig, 0.75mm Spacing and 1800 rpm	55
40 Cone Geometry	58
41 Geometry of Connecting Cylinder.....	59
42 Geometry of Lovejoy Coupling Joint	60
43 Installation of the Cone.....	74
44 Installation of the Shell.....	75
45 Installation of the Cone and Shell.....	76
46 Installation of the Tapered Bottom Bearing.....	76
47 Installation of Nut and Set Screw	77
48 Installation of Rectangular Joint	77
49 Installation of Lovejoy Coupling.....	78
50 Installation of Shivel Screw to the Spacing Controller Cylinder.....	78
51 Installation of the Reactor Assembly to the Motor.....	79
52 Emergency Shutdown Button	81
53 Feed Inlet	82
54 WJ 200 Series 3Phase Inverter	83
55 Pressure Gauge, Pressure Regulator and Switch	84
56 Flange, Product Outlet and Metallic Handle.....	85
57 Nuts and Bolts of the Reactor	86
58 Outlet Temperature for Different Holdup Time at 0.75mm Spacing, 1210 RPM 100 psig Feed Pressure (Corresponding Plot of Table 14)	89
59 Outlet Temperature for Different Holdup Time at 1mm Spacing, 1210 RPM and 100 psig Feed Pressure (Corresponding Plot of Table 15)	90
60 Outlet Temperature for Different Holdup Time at 1.25mm Spacing, 1210 RPM and 100 psig Feed Pressure (Corresponding Plot of Table 16)	91
61 Outlet Temperature for Different Holdup Time at 0.75 mm Spacing, 1800 RPM and 100 psig Feed Pressure (Corresponding Plot of Table 17)	92
62 Outlet Temperature for Different Holdup Time at 0.75mm Spacing, 1505 RPM and 100 psig Feed Pressure (Corresponding Plot of Table 18)	93
63 Outlet Temperature for Different Holdup Time at 0.75 mm Spacing, 1210 RPM and 100 psig Feed Pressure (Corresponding Plot of Table 19)	94
64 Outlet Temperature for Different Holdup Time at 0.75 mm Spacing, 912 RPM And 100 psig Feed Pressure (Corresponding Plot of Table 20)	95
65 Outlet Temperature for Different RPM at 0.75 mm Spacing, 180 seconds Holdup Time and 100 psig Feed Pressure (Corresponding Plot of Table 21)	96
66 Outlet Temperature for Different RPM at 0.75 mm Spacing, 120 Seconds Holdup Time and 100 psig Feed Pressure (Corresponding Plot of Table 22)	97
67 Outlet Temperature for Different RPM at 0.75 mm Spacing, 60 Seconds Holdup	

Time and 100 psig Feed Pressure (Corresponding Plot of Table 23)	98
68 Outlet Temperature for Different Spacing at 180 Seconds Holdup Time, 1210 RPM 100 psig Feed Pressure (Corresponding Plot of Table 24)	99
69 Outlet Temperature for Different Spacing at 120 Seconds Holdup Time, 1210 RPM and 100 psig Feed Pressure (Corresponding Plot of Table 25)	100
70 Outlet Temperature for Different Spacing at 60 Seconds Holdup Time, 1210 RPM and 100 psig Feed Pressure (Corresponding Plot of Table 26)	101
71 Tachometer Reading (RPM) vs. Frequency.....	104

LIST OF SYMBOLS

C_p	Specific heat capacity, J/kg K
F	Volume force vector, N/m ³
F_r	Volumetric force component radial direction, N/m ³
F_φ	Volumetric force component rotational direction, N/m ³
F_z	Volumetric force component axial direction, N/m ³
k	Thermal conductivity, W/m K
p	Pressure, Pa
Q	Heat source, J
Q_{vh}	Viscous heat, J
r	radius, m
t	Time, s
T	Absolute temperature, K
u	Velocity, m/s
u'	Radial velocity, m/s
v'	Rotational velocity, m/s
w'	Axial velocity, m/s
w_w	Velocity component in angular direction, m/s
W_p	Pressure work, J
<i>Greeks</i>	
ρ	Density, kg/m ³
η	Dynamic viscosity, Pa.s
ω	Angular velocity, m/s
Θ	Temperature
η	Efficiency
γ	Shear Rate

Superscript

T	Transpose
---	-----------

Subscript

t	tangential
a	axial
i	inlet
o	outlet

CHAPTER I

INTRODUCTION

Diarrheal diseases kill approximately 1.3 million people annually, most are children aged 0-4 years (World Health Organization 2004). Contaminated water, as a result of poor or inadequate sanitation, accounts for substantial mortality and is the leading cause of diarrhea in developing countries; especially urban slums. In addition, the 3.5% annual urban population growth rate in developing nations challenges and limits the safety of the drinking water supply (Schertenleib 2004). Fecal matter carrying pathogens can enter the water supply in multiple ways: storm water runoff, septic tank leakage, sanitary sewer system breakage and overflow, and improper disposal of human and animal waste (Santo Domingo 2007).

Parasites that spread throughout the environment with human feces due to poor sanitation include helminthes and protozoa, with particular interest focused on *Ascaris lumbricoides*, *Giardia intestinalis*, *Trichuris trichiura*, *Cryptosporidium spp.* and *Taenia spp* (Tronnberg et al. 2010). Children age 2 to 12 are the target victims of *Trichuris trichiura* and *Ascaris lumbricoides* (Smith 2001). In areas where sanitation is non-existent or ineffective (Tronnberg et al. 2010), these parasites and protozoa cause diseases such as, cholera, diarrhea and typhoid. The helminthes (parasitic worm) infections in the human stomach caused by the microbes listed above are ascariasis, truchuriasis (whipworm), and hookworm. These diseases cause both physical harm and reduce scholarly and cognitive development (Bethony et al. 2006). We are evaluating the concept of viscous heating to define sanitation applications. Similar devices for non-fecal

applications have been reported. Yesilata (2002) worked on the rotation of mass between two parallel disks. We have generated heat from both animal feces and fecal simulants by applying shear stress with extruder types of equipment. Heat has been sufficient to sanitize the mass. For watery solids paper, sawdust or grass clippings could potentially be added to increase viscosity. Alternatively, allowing water in the heated mass to vaporize and then recycling the solids may achieve sufficient temperature rise. Once treated, the feces will be safe to handle or transport and can subsequently be used in energy conversion or agricultural processes.

Preliminary design was evaluated using Computational Fluid Dynamics (CFD). These simulation programs have the ability to solve and analyze energy and mass balances within any geometry. For the case of a shear reactor, these equations describe the mass flow and temperature profiles. CFD is superior to simplified assumptions; such as, one-dimension flow analysis methods using hydraulic radii and lubrication approximations, which are required with traditional approaches (Gifford 1996). CFD results gave the initial geometries specifications prior to construction, which, in turn, reduced significant mechanical trial and error.

1.1 BACKGROUND

Viscous heating is a well-known phenomenon; technologies include polymer melts and sludge dewatering. Rock formation is also associated with viscous heating in nature. A discussion of the contribution of viscous heating in the field of geology, along with modeling of the effects is presented by Burg (2005), while the contribution of viscous heating in magma deformation is studied by Hess (2008)

In viscous heating, temperature rise is caused by internal friction at high flow velocities (Sunden, 1992). Sunden showed viscous heating effects in forced convective flow across a circular

cylinder at low Reynolds numbers. To evaluate viscous heating for this application fecal simulants were used. Structural, thermal, and viscoelastic properties for potatoes (Singh et al. 2008) indicate their potential as a simulant. Yavuz et al. (2011) investigated laminar duct flow heat transfer with viscous dissipation for a Newtonian fluid to define temperature distribution within annular pipes. Finite difference analysis of the heat transfer mechanisms for non-Newtonian fluids in circular tubes showed that viscous dissipation leads to high temperature in processing fluids. Heat generated decreases the viscosity of the fluid and results in less temperature rise than for a material with constant viscosity (Costa and Macedonio 2005).

Hooman and Ejlali (2010) included viscous heating in a correlation to improve flow simulation. They explained liquid viscosity decreases with incremental temperature which results in lower pressure drop. Although they provided a theoretical solution for both no-slip and slip flow in cases with forced convection of liquid in a micro channel flow, no experimentation was included. However, an analytical solution for nonisothermal flow with wall slip provides a better understanding of temperature rise in die flow for viscoelastic fluids (Lawal and Kalyon 1997). Since the mathematical solution indicates the ability to measure the accompanied viscosity and this analytical solution has the advantage of application over a varied range of viscoplastic fluids. Depending on the resultant viscosity, a portion of the processed product might be recycled to sustain constant viscosity. Temperature distribution due to viscous heating is discussed by Collins (1983).

Whipworm, *Trichuris trichiura*, is found in the cecum, appendix, colon and rectum of infected people (Capitola, 2012). Research shows that whipworm is common in moist, shaded, and warm tropical and subtropical areas of the world. This parasite infects children of all age groups. People infected by whipworm may suffer from diarrhea, Anemia, abdominal pain, nausea, vomiting, tenesmus, and rectal prolapse (Cross 1996). Estimates are that up to 800 million infections occur by the eggs in contaminated soil, foods, or drink. A female *Trichuris trichiura*

produces 2,000 to 10,000 eggs per day which passes in the feces and spreads in the environment. Once ingested by food or drink, embryonated eggs hatch and mature. Matured females start laying eggs within 3 months after infecting the host (Cross 1996).

The eggs generally take 70 days to mature. Diseases related to *Trichuris trichiura* include diarrhea, anemia, and dehydration. This microorganism is also found in cats throughout the United States. The eggs hatch and the larvae mature as adults nourishing on the blood in the large intestine wall. The matured organisms lay eggs which are carried by the feces of the infected individual to the environment where they can survive in soil for years. Examining either the feces or blood in the feces allows the organisms to be detected. Bundy et al. (1985) studied *Trichuris* and *Ascaris* in Jamaica and found more people are susceptible to *Trichuris*. The cognitive response in children was also shown affected (Nukes et al. 1992).

1.2 OUR PROPOSAL

Developing a Shear Reactor Assembly That Treats Fecal Wastes

Section I. The objective of this project is to develop a device that can rapidly disinfect and dewater wet, solid human and animal waste. Shear reactors that force mass through a small opening (die) generate significant heat and pressure. Commercial devices of this type are commonly referred to as extruders and are used effectively to melt plastics, cook grains and dewater solids. The die is basically a small plug-flow reactor that generates its own heat from friction as a result of mass being forced through a restricted opening at high pressure. Upon leaving the die the high pressure is relieved and any moisture is vaporized and released as steam. For example, in the case of corn extrusion, the solid that remains has the appearance and texture of cooked corn chips. The temperatures and pressures observed within the die are sufficient to destroy microorganisms; however, the additional mechanisms of shear stress moving through the die and pressure shock as steam escapes upon leaving also contribute to microbial destruction.

The result of combining all three mechanisms is that extruders have the potential to be highly effective in sterilizing wet, solid waste. The effectiveness of the device depends on several variables including temperature, pressure, residence time within the die (die geometry, rheological behavior and mass flow rate), moisture content, and rotational speed of the reactor core. Pistons can also be used in place of augers to force mass through a die, but may be more complicated to operate.

This idea may be considered unconventional because it extends well-known extrusion technology to the treatment of human and animal wastes. More importantly, the technology is able to address the solicitation requirements. The device would require no water or chemicals to operate effectively; in fact, low water content is highly desirable to maintain high viscosity. When constructed of quality materials the shear reactor components would have a long, useful life with little or no maintenance. The use of a motor to power the device is anticipated, but a hand- or foot-cranked version may be possible if the required torque can be achieved through a geared mechanism (envision the rpm achieved by an old fashioned, hand-cranked, batter mixer). The size may be small: a hand portable device could address the needs of a single user or small group, while one capable of treating the waste of a small community could be the size of a small trash canister. In either case, the devices can be used effectively as independent, decentralized units. Small size also allows them to be private, discreet and easily moveable without drawing attention. Small device size also allows for easy replacement in the case of failure. The device would work quickly, within a matter of seconds, thereby minimizing odors and attraction to flies as compared to waste left untreated for hours or days. The water removed from the waste will leave as steam; and, if condensed, would be a relatively clean water source that should be evaluated for agricultural or other uses. Due to the dewatering process the solid mass to be disposed will be of reduced volume, thereby resulting in easier and safer handling and movement, if required. The existence of paper or fiber from tissue or menstrual supplies mixed within the feces is not

expected to affect the performance of the device, and may be an aide in retaining the desired viscosity. The extruder is expected to work equally well with feces from both adults and children.

Section II. The concept is simple: forcing mass through a die results in increased temperature and pressure that dewater waste while destroying microorganisms. The detailed design requires development, testing and optimization. Step 1 is to perform a preliminary design using Computational Fluid Dynamics (CFD) to define effective system variables: mass flow rate, cone torque of the reactor and geometry and die dimensions. From these inputs, CFD can determine temperature and pressure gradients and mass residence time within the die. The objective is a device that is simple, easy to use and understand; yet can operate optimally to sanitize the input material. There are numerous design and operational factors to be considered. An example issue to be addressed is that a device that is not operating continuously may take the die several seconds for the friction to induce sufficiently high temperatures and the possibility that electric resistance or use of a lighter may be required to preheat the die. Another example issue is to define the effective viscosity ranges of the feces; and, if there are limitations, interchangeable die designs that allow the treatment over a wide range. Step 2 is to build a bench scale unit based on the CFD results. Step 3 is to test the unit with model materials and microorganisms in order to compare and refine the CFD simulations and address simplicity and ease of use. Experimental validation should include temperature-time studies, percentage moisture change, viscosity issues, microbial destruction effectiveness and reliability studies. A detailed chemical analysis of both the steam and the solids can be used to determine whether the separate streams have potential value. If experimental data indicate that a modification of the design is required, then Step 4 is to build a second, more effective, prototype. Step 5 is to test the device on natural materials.

The performance data generated during Phase I will lead to effective shear reactor geometry with defined and proven operating ranges. Data will include extruder effectiveness at reducing and eliminating microbes in both model and natural test samples. Whether a motor is required or

whether a hand-cranked device is possible will be determined. Ease of operation, aesthetics and cultural factors will be important considerations in evaluating the device performance. Data will be sufficient to determine project viability and whether further investment is reasonable. While it is anticipated that different size extruders will be required for different applications, during Phase I only a laboratory-sized device will be developed and tested.

Phase II objectives will address evaluating the technology in practice. These devices can be placed in the field and evaluated to define their actual effectiveness, ease of use and acceptability. Not only will technical performance data be collected and evaluated, but the more general aspects of people utilizing the technology will be a significant component of Phase II. These types of questions include acceptance of the technology by individuals and communities, ease of understanding and use of the device and identifying to what degree waste extruders are capable of improving the quality of life for those that use them.

CHAPTER II

COMPUTATIONAL FLUID DYNAMICS

2.1 GOVERNING EQUATIONS

Typically, an extruder-die design depends on three elements, an accurate viscosity model, ability to solve 3-dimensional flow equations and an objective function to distinguish among designs. An accurate flow prediction requires an accurate viscosity model that includes the effects of shear rate. When the viscosity correlations are unknown, the designer must define appropriate equations prior to model development. For example, most polymers behave as a Newtonian fluid at low shear rates; however, they become shear-thinning fluids under high shear force. A flow analysis requires a continuous viscosity correlation extending over the full shear-rate range observed in the analyzed fluid. The applicability of a model depends on the representation of the experimental data. When a power-law expression is not adequate, a more suitable model, such as those by Carreau-Yasuda, Bird-Carreau and Cross, may be required (Gifford 1996, Vlachopoulos 2003).

Comsol Multiphysics v4.2a (C-M) – a commercial CFD package – can be used to analyze the temperature profile within the reactor geometries (COMSOL MULTIPHYSICS 2011). C-M can handle steady state, transient flow with heat equations using finite element algorithm in both two-dimensional and three-dimensional geometries.

The flow is governed by the time-dependent Navier-Stokes equation. Equation 1 represents the vector form of the conservation of momentum and Equation 2 is the continuity equation for the conservation of mass. The heat transfer in the fluid domain is described by equations 3 through 5.

$$\rho \left(\frac{\partial \mathbf{U}}{\partial t} + \mathbf{U} \cdot \nabla \mathbf{U} \right) = -\nabla p + \nabla \cdot \boldsymbol{\tau} + \mathbf{F} \quad (1)$$

$$\nabla \cdot \mathbf{U} = 0 \quad (2)$$

$$\rho c_p \left(\frac{\partial T}{\partial t} + \mathbf{U} \cdot \nabla T \right) = \nabla \cdot \mathbf{q} + \dot{q} \quad (3)$$

$$\mathbf{q} = -k \nabla T \quad (4)$$

$$\boldsymbol{\tau} = \mu \left(\nabla \mathbf{U} + \nabla \mathbf{U}^T \right) - p \mathbf{I} \quad (5)$$

The terms Q_{vh} and W_p are added to the general heat-transfer equation to include viscous heating and pressure work effects. The design is created using 2-dimensional axisymmetric geometry. Since the geometry is rotationally symmetric, it can be modeled as a 2D cross section (Figure 1).



Figure 1. Design Model Setup and Boundary Conditions

All three velocity components must be included in the model since the velocities in the angular direction are different. The flow equations (6 through 8) for a stationary axi-symmetric geometry are described Gresho and Sani (1998):

$$\rho \left(u' \frac{\partial u}{\partial r} - \frac{v'^2}{r} + w' \frac{\partial u}{\partial z} \right) + \frac{\partial p}{\partial r} = \eta \left[\frac{1}{r} \frac{\partial}{\partial r} \left(r \frac{\partial u'}{\partial r} \right) - \frac{u'}{r^2} + \frac{\partial^2 w'}{\partial z^2} \right] + F_r \quad (6)$$

$$\rho \left(u' \frac{\partial v'}{\partial r} + \frac{u'v'}{r} + w' \frac{\partial v'}{\partial z} \right) = \eta \left[\frac{1}{r} \frac{\partial}{\partial r} \left(r \frac{\partial v'}{\partial r} \right) - \frac{v'}{r^2} + \frac{\partial^2 v'}{\partial z^2} \right] + F_\phi \quad (7)$$

$$\rho \left(u' \frac{\partial w'}{\partial r} + w' \frac{\partial w'}{\partial z} \right) + \frac{\partial p}{\partial z} = \eta \left[\frac{1}{r} \frac{\partial}{\partial r} \left(r \frac{\partial w'}{\partial r} \right) + \frac{\partial^2 w'}{\partial z^2} \right] + F_z \quad (8)$$

For this model the volumetric force components F_r, F_ϕ and F_z are set to zero. On the inner cylinder wall, a sliding wall boundary condition is used to specify the velocities. The velocity components in the plane are zero. The velocity components in the angular direction are computed by equation 9.

$$w_W = r\omega \quad (9)$$

2.2 ANALYSIS OF GEOMETRY

We describe how CFD is used to devise a shear reactor that would disinfect human feces by performing a variable analysis. Once experimental data have been collected the CFD can be fine-tuned for additional analysis. The geometry of the reactor is rotationally symmetric and can be modeled as a 2D cross section (Figure 2). At the outer cylinder wall a no-slip condition applies. The outlet is set to atmospheric pressure and inlet velocity is specified at the inlet boundary in z direction. The initial conditions of 0 Pa and 293.15 K are used. The inlet temperature is maintained at 293K. An Open Boundary node with an exterior temperature of 293K is used for

the outlet, although a non-uniform temperature distribution is expected (Dinh 1982). The angle of the extruder is chosen to allow multiple spacing tests with a single experimental device. By fixing the shell and moving the core axially the spacing can be adjusted. Use of an angle for a final device is not anticipated.

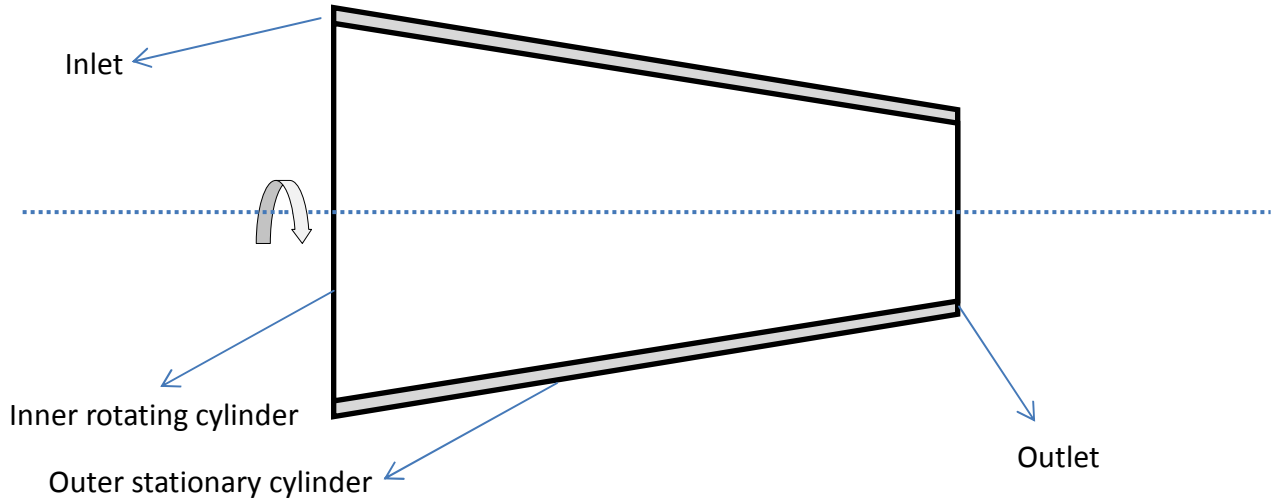


Figure 2. Reactor Geometry Used for CFD Studies

The geometry is meshed using an interactive technique. A total of 210 triangular elements are created within a mesh area of $1.0 \times 10^{-4} \text{ m}^2$. Table 1 shows the fluid properties assumed in this study. The simulations were performed with stationary Fully Coupled solver configuration. A Parallel Sparse Direct Solver (PARDISO) was used to obtain simulation results.

Table 1. Assumption of Fluid Properties to Simulate in CFD

Density, ρ	1000 kg/m ³
Viscosity, μ	5 Pa.s
Thermal conductivity, k	0.03 W/(m.K)
Heat capacity, C_p	4186 J/(kg.k)

CHAPTER III

RHEOLOGY AND OTHER PHYSICAL PROPERTIES

3.1 EXPERIMENTAL METHOD

In order to measure the viscosity of different types of potatoes and wheat flour, we used a rheometer from Bohlin Instruments Model CVOR 200, East Brunswick, NJ (Figure 3). A sample was placed in a plastic cup within a ball mill of a THINKY grinder from Phoenix Equipment, Rochester, NY to create a paste. A 2.5 ml sample by syringe was passed inside the serrated cylinder within the rheometer. The experiment was performed at a 150-micron gap and 40°C.



Figure 3. CVOR Bohlin Rheometer

First the sample whose viscosity would be measured was taken in a plastic cup with some balls (Figure 4). Sample was kept in the white cup (left of figure 4) and polymer balls (left of figure 4) were added. The cup was weighed to keep the weight within certain limit. Weighing was performed to achieve proper rotation of the cup in the grinder.



Figure 4. Plastic Cup (left) and Balls (right) for Grinding Feed

The cup with the sample was placed inside the grinder from Phoenix Equipment, Rochester, NY model name Thinky (Figure 5). The sample was grinded for one minute and uniform paste produced in one minute. The Thinky grinder could automatically be switched off after one minute of rotation.



Figure 5. Thinky Grinding Machine

With a syringe 2.5 ml of sample was collected from the cup and passed inside the serrated cylinder (left of Figure 6) of the rheometer. The cylinder was hammered on a rubber pad to settle down the paste inside the cylinder properly and confirmed that no bubbles existed. The rheometer was set to zero after turning on. The user must calibrate the viscometer before using it every time. The calibration includes making the gap zero and then setting to desired gap. In our experiment, the gap was 150 micron. The rotating shaft screw (right of figure 6) was set for rotating inside the serrated cylinder while performing the rheology experiment.



Figure 6. Serrated Cylinder (Left) and Rotating Shaft (Right)

A black rubber is always put around the cylinder (Left of Figure 7) mouth and water added on the edge to keep the moisture content of the sample constant during the experiment. In addition, two half circular shape plastic plates (right of Figure 7) are used to close the head of the serrated cylinder. The half circular plates are kept wet with soaked filter papers. This arrangement compensates for any moisture loss from the sample.



Figure 7. Black Rubber (Left) and Plastic Semi-Circular Plate with Filter Paper (Right)

Once the arrangement is ready with the sample inside the cylinder, the arrow was pushed to enter inside the serrated cylinder (left of figure 8). When the rotating shaft enters inside the serrated cylinder, the black rubber and the semi-circular plastic plates are placed. The final Setup is shown in the right of Figure 8.



Figure 8. Final Setup for Viscosity Measurement

A heating system from PolyScience of Niles, Illinois (Figure 9) is used to maintain the temperature during the experiment. The heating system is a separate unit which works to cool or heat the sample circulating water around the serrated cylinder containing sample. The metallic

body of the serrated cylinder is conducive to transfer heat efficiently. Most of our experiments were run at 40°C.



Figure 9. Poly Science Water Circulating Heating System

The Computer attached to the rheometer was turned on and Bohlin shortcut was clicked. The software for Bohlin instrument was launched. By clicking viscometry and typing the desired temperature, experiment was begun (Figure 10).

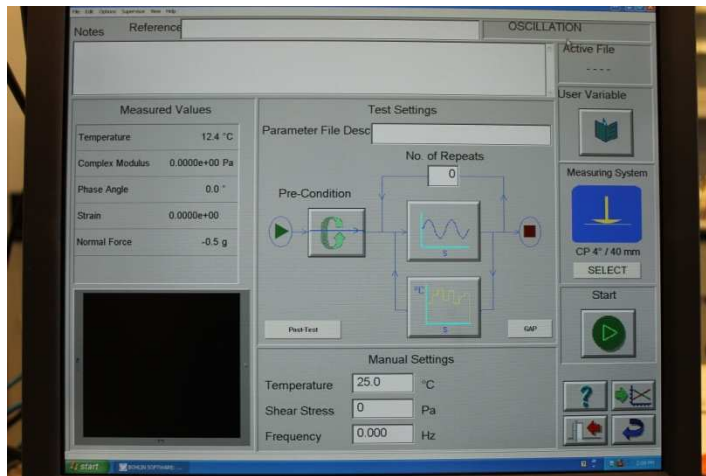


Figure 10. Computer Demonstration for Viscosity Data Gathering

Near the upper left corner, an icon shows the temperature rise over time. This is due to circulation of hot water around the serrated cylinder to reach desired temperature set by the user. When the desired temperature is achieved, start button was clicked to begin experiment. Between the upper

middle and upper right corner, a clock showed up indicating that how many minutes (time) were remaining to finish the experiment. In our experiments, the time required for each run was near about 25minutes. At end of the each experiment, a menu showed up. Data are saved by clicking “OK” for future use.

3.2 FAKE STOOL PREPARATION

Fake stool was prepared by mixing rice, soybean paste, salt, and water. The composition of fake stool is given in table 2 (Sanitation Network Science & Technology, 2012). Boiled rice was weighed by a digital scale from Ohaus Corp, Pine Brook, NJ and salt was added proportionately. A uniform and soft paste was produced by grinding the mixture for one minute in the THINKY grinder. The soy bean paste was weighed and ground using the same technique and added proportionately to the previous salt-rice paste. The solution was heated and mixed in a beaker and excess distilled water was added to allow sufficient vaporization (Figure 11). A 110 gm mixture was prepared. The paste was heated and stirred for twenty minutes at 90°C. After twenty minutes, the temperature of the heater was increased to about 150°C and the condition was sustained for about ten minutes to boil up the mixture and confirm that no granular particle existed. We followed a two-step heating protocol (up to 80-90°C and then to 150°C) to avoid burning the mixture when subjected to 150°C directly.

Table 2. Composition of Fake Stool

Ingredient	Percentage
Salt	12.2
Rice	18.5
Soy Bean Paste	33.8
Water	35.5

Numerous bubbles were observed from the upper surface of the mixture. The mixture was weighed every two or three minutes. When lesser weight was observed, less than 100 g, 5-10 ml

water was added. The mixture was stirred continuously during the entire experiment. The sample was allowed to cool to room temperature. We performed rheology experiments with the final mixture.



Figure 11. Fake Stool Preparation

Results show that starch from potatoes and flour resembles the viscous properties of fecal matter. Figure 12 presents viscosity data for pig caecal, chicken caecal, and human stool compared with several starchy materials and fake stool (Doucleff 2012). The graphical representation for fecal matter follows a trend line similar to potato and flour except for potato starch. Similar plot would be found for wheat and maize starch paste in Ellis (1989). Based on these data, we selected red potato as our fecal simulant. To prepare feed to operate the extruder, red potatoes were boiled for at least one hour. After 10-15 minutes, the skin was removed and potatoes were mashed in a ricer. For both slip and no slip condition were tasted for red potato. No significant difference was observed.

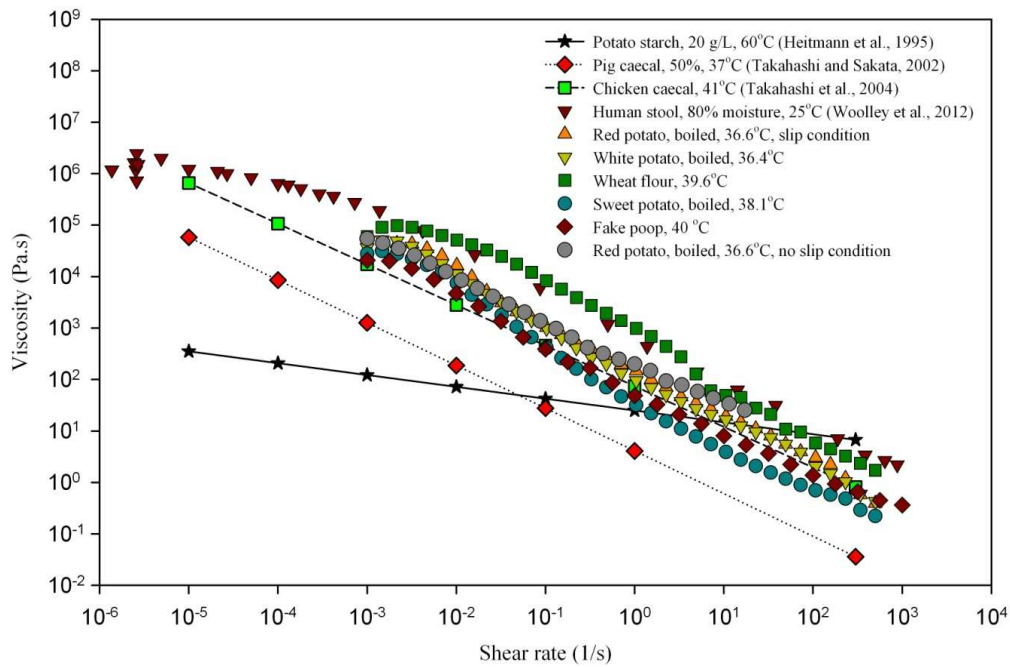


Figure 12. Shear Rate Decrease with Viscosity for Various Feces and Simulants

3.3 MOISTURE CONTENT OF POTATO

Moisture content of potato was determined by weighing weight and volume of the potato sample.

The paste was dried for two different drying periods. Red potato boiled, peeled and cut into pieces. A small piece was taken on a Petri dish and weighed. The piece was dried for about 6 hours in an oven at 35° C and again weighed. The moisture content was calculated from the values of initial weight and final weight.

Table 3. Moisture Content in Pieced Boiled Potato after 6 Hours of Drying at 35° C

Initial Weight gm	Final Weight gm	Moisture Content %
4.2860	2.1666	49.44
5.2632	2.2763	56.75
5.0162	2.4009	52.14

Red potato was boiled, peeled and mashed. Small amount of past was taken on a Petri dish, spread over it and weighed. The paste was dried for about 22 hours in the same oven at 45° C and again weighed. The moisture content was calculated from the values of initial weight and final weight.

Table 4. Moisture Content in Boiled Mashed Potato after 22 hours of Drying at 45° C

Initial Weight	Final Weight	Moisture Content
gm	gm	%
3.5004	0.7801	79.43
4.858	0.9716	77
4.8896	1.0978	77.54

As can be see, from the table 3, the moisture content of potato is much lower than that of the values of given in table 4. This is because of not mashing the potato in the case of first set of data. The surface area for drying was significantly lower in first trial. Drying was faster for the readings of table 4, as potato was mashed and spread over the Petri dish. Also drying period was fourth times for these values in comparison to the values mentioned in table 4. We have assumed moisture content as 80% for entire calculation in this thesis.

3.4 DENSITY OF POTATO

Density of potato was determined in two ways-before and after boiling. The purpose was to determine whether there is any contribution of boiling on density and calculating the volume processed in the gap of the shell and cone of the reactor. Raw red potatoes were peeled and cut into rectangular shape so that they can be fit into a 15 ml cylindrical flux.

The flux was filled with small amount of water, placed on a digital weighing scale from Fisher Scientific, Ohaus Corp. Pine Brook, NJ (Figure 13) and tarred off. The volume reading of water in the cylinder was recorded from the calibration of the flux. The pieced rectangular potato was placed inside the cylinder and again volume reading taken. The weight of the piece of the potato

was recorded up to four decimal points with the help of the weighing scale. Data were taken three times for raw potato. Using the volume and mass reading density of potato was calculated before boiling.



Figure 13. Digital Weighing Scale from Fisher Scientific

The data are given in table 5. For determining the density, potato was boiled. The skin of the potato was removed and cut into small pieces. One small piece was taken and experiment was performed similar to that of the density determination of the raw potato. The data taken are shown in table 6.

Table 5. Density Determination of Red Potato before Boiling

Initial Volume	Final Volume	Difference of Volume	Weight	Density	Average of Density
ml	ml	ml	gm	gm/cm ³	gm/cm ³
5	6.9	1.9	1.9924	1.0486	1.045
4	5	1	1.0298	1.0298	
7	9.3	2.3	2.4299	1.0565	

Table 5 and 6 display mean density determined for red potato before and after boiling. The result from table 6, we have mean density of potato 1.0796 gm/cm^3 is greater than the density mentioned in table 5, which is higher to some extent. This indicates that the density of potato increases because of boiling.

Table 6. Density Determination of Red Potato after Boiling

Initial Volume	Final Volume	Difference of Volume	Weight	Density	Average of Density
ml	ml	ml	gm	gm/cm^3	gm/cm^3
5.2	6.2	1	1.0292	1.0292	1.0796
3.2	3.8	0.6	0.6685	1.1142	
6.2	8	1.8	1.9717	1.0954	

Water enters inside cells of potato and increases the volume of the potato. This contributes to increase in density of boiled potatoes. While boiling submerged into water, the potato absorbs a little amount of water which increases the final volume of the potato flakes.

CHAPTER IV

EXPERIMENTATION WITH SIMULANT

4.1 FEED PREPARATION

Take two red potatoes in a stainless steel stock pot and fill the pot with enough water so that, the potatoes can be boiled more than thirty minutes completely submerged in water. Place the pot onto the stove. Turn the switch on. Wait at least thirty minutes and thoroughly boil the potatoes. It is important to note that at the end of boiling, the potatoes must be soft from all sides of its crust and there are no hard or coarse parts in the potatoes. The best preparation will be when there is cleavage in the skin of the potatoes after rigorous boiling of at least one hour. This is to achieve appropriate density of the potatoes. It is advised not to microwave the potatoes. Microwaved potatoes have harder and coarse crust which would be difficult to be processed through the reactor.

When the skin of the potatoes is cleaved properly, turn off the stove and collect the potatoes with ladle from hot water. Allow ten to fifteen minutes to let the potatoes to be cooled at room temperature. Then remove skins completely from all the potatoes. Take a ceramic bowl and grind the potatoes with a potatoes masher properly (Figure 14). When mashing is done, test with hand whether there is any bigger or coarse particle. In case of course piece found, mash the potato again.



Figure 14. Mashing Potatoes with Masher

Take the mashed potatoes in a potatoes ricer and make a uniform paste of potato (Figure 15). Perform this task twice recycling back the riced potato. The uniform paste is ready to charge in the reactor.



Figure 15. Making Smooth Paste with Ricer

4.2 OPERATING TECHNIQUES

Our first generation viscous heating unit is shown in figure 16. The machine operates with a variable pressure (0-100 psig) for feed rate control, spacing (0.75-1.25mm) between the rotating inner core and the fixed outer shell (type 304 stainless steel was used to build the core and shell) and rotations per minute (rpm) (0-1800). For typical operation, the room temperature is assumed constant and feed occupies the spacing completely. The simulant mass is placed inside the feed

chamber, the spacing is adjusted, pressure and rpm are set and the extruder is activated. An electric switch opens the air valve and moves the plunger that pushes simulant or feces into the gap. Once some initial mass was observed to exit the shell, a rubber stop cork was used to close the outlet for a time (hold up time) to allow the equipment and the mass to heat due to friction. After the desired temperature is achieved the stopcock is removed and mass flow is established. The mass in the annular space has a defined holdup time. During experimentation temperature is recorded by a thermocouple; an Omega HHM 31 Digital Multimeter and rpm by a digital photo laser tachometer (Non Contact). Air pressure, spacing, rpm, and torque data are collected.



Figure 16. Instrumentation on Reactor to Process Fecal Sludge and Simulant Solids

The plunger on the left in figure 3 moves inside a cylindrical feed chamber to press the feed inside the shell. A hole on the cylindrical chamber allows the operator to charge the feed. The plunger is air driven and can push the feed with a gauge pressure from 0 to 100 psi. In the figure, the pressure gauge is hanged on the metallic vertical wall. Below the gauge, the yellow regulator

controls the pressure. On the right side of figure 3, a Hitachi WJ200 Series 200 V three-phase inverter is attached on the vertical wall to set the required rpm of the AC motor. The shaft from the motor is connected with the cone stem by a Lovejoy coupling joint. The rpm is set on the digital panel. An emergency button is fixed on the vertical wall in order to stop the operation suddenly.

The cone and the shell are shown in figure 17. The fixed shell has a spacing calibration ranging from 0 to 1.25 mm. The cone moves inside the shell. In contact with the inner cone surface, mass starts rotating, deforms, and creates friction. The moveable bearing is attached around the stem of the cone with a black circular plastic rubber seal. The combination aligns the cone in a concentric position inside the cylindrical shell. The black hole shown on the shell in figure 4 serves as an outlet. The bore size is 0.32 inch² or 2.1 cm². The shell was calibrated for three positions: 0.75, 1.00 and 1.25 mm.



Figure 17. The Cone (left) Rotates inside the Housing (right)

The assembled components are presented in figure 18. Spacing between the rotating cone and the stationary shell (right side in figure 18) is fixed by the operator. A handle is moved to set the desired spacing based on the calibration. The spacing between the housing and rotating shaft is increased if the metal handle is pushed forward to the vertical metal wall (anticlockwise direction as you look at from the side of air cylinder (inlet)). A detail installation and operating procedure are given in appendix A and B.



Figure 18. A Typical Setup of the Cone inside the Housing with Spacing Controller and Outlet
Cork (Black)

We used a Bio-safety Level 2 (BSL-2) laboratory in the National Center for Veterinary Parasitology at Oklahoma State University to perform tests on baboon feces infected with *Trichuris trichiura*. Since the baboon population is treated for this infection on occasion, the organism loading levels were quantified by observation under microscope. This analysis requires a sample of known mass placed in water, gently agitated to allow parasite eggs to float to the surface. Following the same procedure as used for simulants, the feces was placed in the extruder

and subjected to viscous heating. After a hold up time from 3 to 4 minutes, to achieve initial heating, the feces were allowed to pass out of the extruder at near steady state as allowed by the sample size. Temperature data were obtained with a thermocouple. Samples of the effluent were collected; remaining eggs were floated and counted under the microscope.

CHAPTER V

RESULTS AND DISCUSSION

5.1 TEMPERATURE GRADIENT OBTAINED FROM CFD

5.1.1 Effect of Dimension

To evaluate the reactor geometry, the radius, length, and clearance were varied to define the effect of dimensions on the temperature gradient. The temperature profiles in figure 19 show an increase in maximum temperature with greater length. Higher temperatures are observed towards the end of the reactor. A maximum temperature of 205 °C is predicted with a 0.1 m reactor length. Increase in reactor length results in greater residence time and increased viscous heating that is a function of surface area.

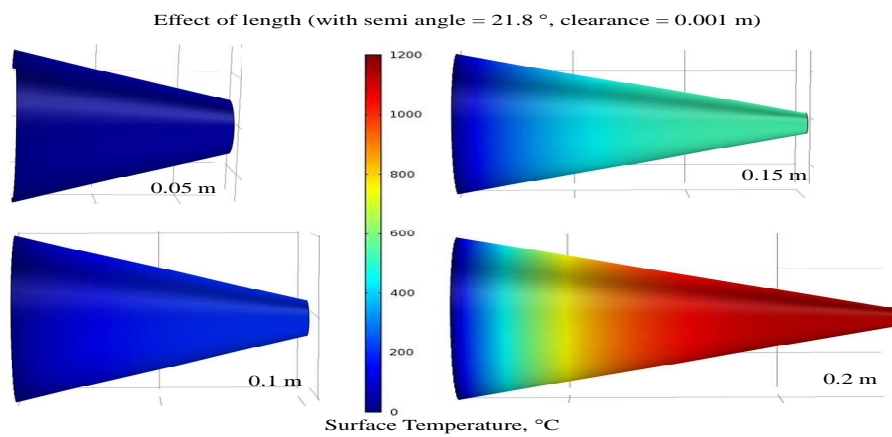


Figure 19. Effect of Length with Semi-Angle = 21.8° and Clearance = 0.001m

The change in the angle of the cone follows the same trend as changes in length (figure 20).
Increasing the angle of the cone increases surface area and viscous heating.

Effect of Semi Angle (with Length = 0.1 m ; Clearance = 0.001 m)

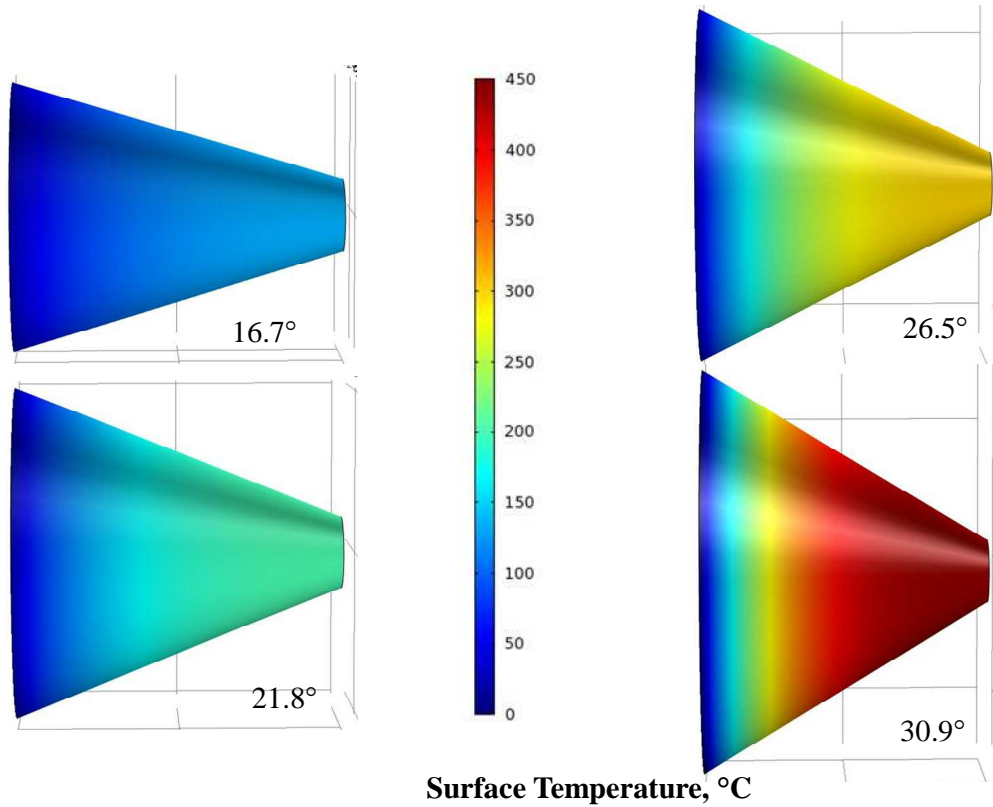


Figure 20. Effect of Semi-Angle with Length = 1 m and Clearance = 0.001 m

A smaller clearance results in higher maximum temperature, a clearance of 0.0015 m will heat the fluid to a maximum temperature of 108°C (figure 21). However, reducing the clearance limits the amount of fluid entering the reactor resulting in increased operating time.

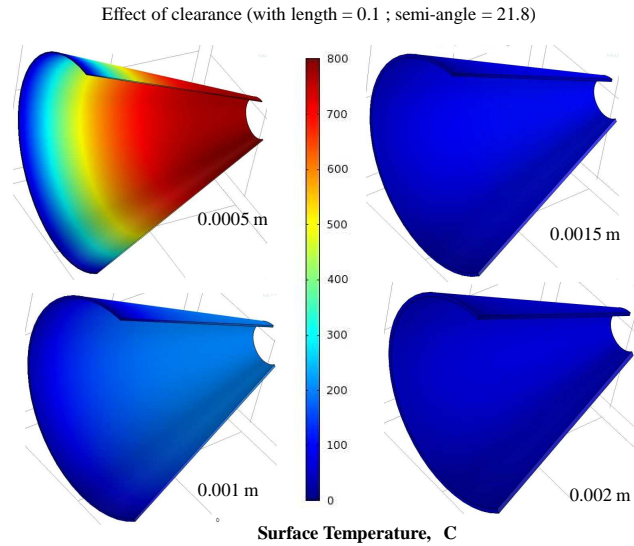


Figure 21. Effect of Clearance with Length = 0.1 m and Semi-Angle = 21.8°

5.1.2 Effect of Inlet Velocity

As inlet velocity decreases, viscous heating increases due to longer residence time. An inlet velocity of 0.002 m/s results in a maximum fluid temperature of 205°C (figure 22). Viscous heating of fluid depends mainly on the angular velocity of the inner cone; higher angular velocity and lower inlet feed velocity are necessary.

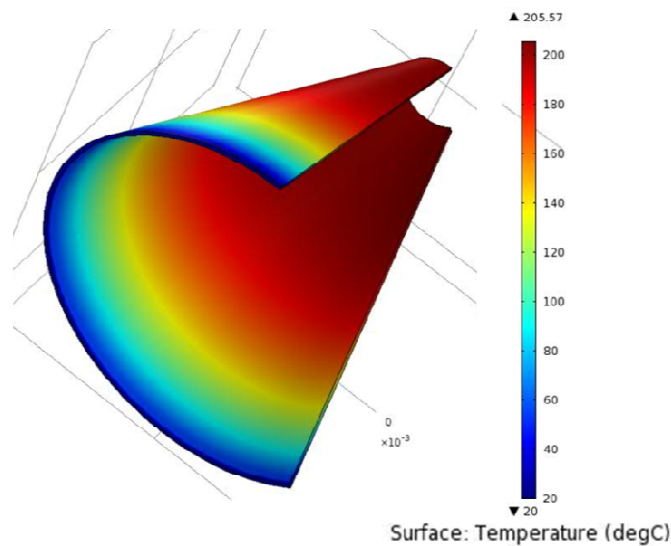


Figure 22. Temperature Gradient with Inlet Velocity 0.002 m/s at 500 rpm

5.1.3 Effect of Angular Velocity

Viscous heating depends significantly on the angular velocity of the inner cylinder. An increase in angular velocity increases viscous heating. A maximum temperature of 205°C is obtained at 500 rpm (figure 22). Higher temperature is observed towards the end of the reactor. The temperature distribution shows an opposite trend to the angular velocity profile. The angular velocity magnitude decreases with decrease in length for the reactor resulting in relatively higher residence time for the fluid towards the end of the reactor. Furthermore, although the feed inlet velocity is higher towards the end of the reactor due to decrease in radius of the cone, the higher magnitude of the angular velocity overcomes the effect of increase in feed inlet velocity.

For a larger diameter the shear rate would be higher as diameter is proportional to the shear rate. But with a larger diameter the surface area of the cone would be increased. As heat transfer to the environment is proportional to the surface area of the metallic surface, this would lead to higher heat transfer to the environment when the surface is not insulated. Further simulation on CFD is required to understand the effect of diameter of the on the viscous heating. An optimized design can be obtained by CFD

5.2 HEAT GENERATION IN SIMULANT (RED POTATO)

As the core rotates inside the housing, the mashed potatoes pass between the two metallic surfaces. The outlet is closed for a certain time and the potatoes gain heat. When allowed to exit the reactor, the elevated temperature observed initially reduces as the mass cools due to water evaporation and release to atmospheric pressure. Table 7 shows data for experiments at 1800 rpm with a spacing of 0.75 mm and feed pressure of 100 psig. As the holdup time increases the temperature increases. Experiments were stopped once the temperature approached 200°C because this exceeded the temperature required to sanitize waste and resulted in more wear and tear on the equipment. The initial temperature (34°C) was due to a previous experiment and residual heat of the metal.

Table 7. Temperature with Time at Constant Feed Pressure, RPM and Spacing

Feed	Feed Pressure	rpm	Spacing	Time	Temperature Outlet
	psig		mm	seconds	°C
Red Potato	100	1800	0.75	0	34
				60	64
				120	74
				180	86
				240	162
				260	190

The temperature increases linearly with the holdup time, indicating that longer holdup time would result in higher temperature. A temperature reading of 190°C was obtained at 260 seconds hold up time. This temperature exceeds that required to kill all microorganisms found in human feces. Figure 10 presents results for experiments with the reactor feed pressure at 100 psig, 1800 rpm and 0.75 mm spacing. We performed additional experiments – not presented – at constant rpm and spacing and found a similar linear trend for each case. The maximum temperature in figure 23 shows the limitations of the equipment.

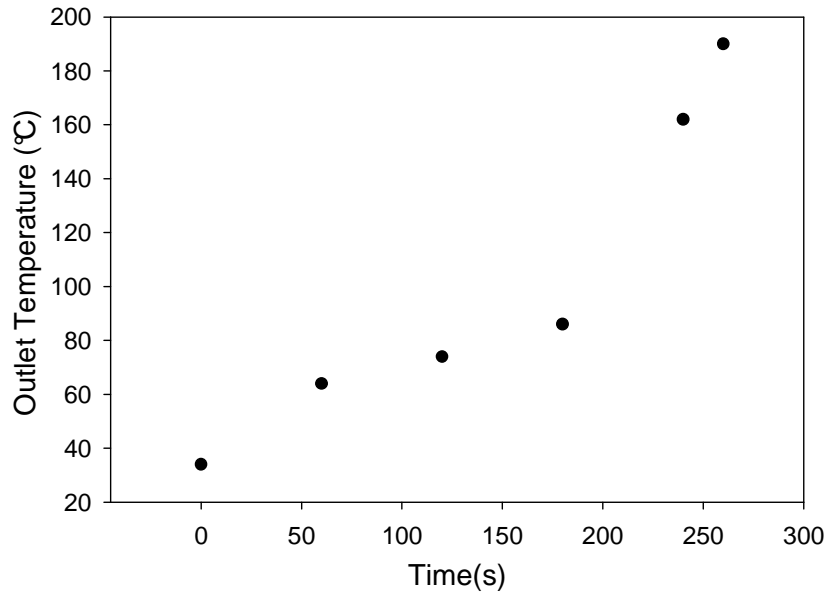


Figure 23. Temperature with Time at 100 psig, 1800 RPM and 0.75 mm Spacing

We believe that increasing rpm and decreasing spacing would continue toward higher temperatures. In table 7 and figure 23 results are presented for constant pressure, rpm, and spacing. Changing these variables for further analysis is possible

Table 8. Temperature Rise with Spacing Change at Constant Pressure, RPM and Time

Feed	Feed Pressure	RPM	Holdup Time	Spacing	Temperature Outlet
	psig		seconds	mm	°C
Red Potato	100	1209	180	0.75	72
				1	70
				1.25	50

Table 8 presents data where spacing is varied while pressure, rpm, and holdup time are held constant. Temperature rise was observed with decreasing spacing. From table 8, temperature decreases with increased spacing. These results indicate the likelihood that lower spacing, less than 0.75 mm, will generated even higher temperature.

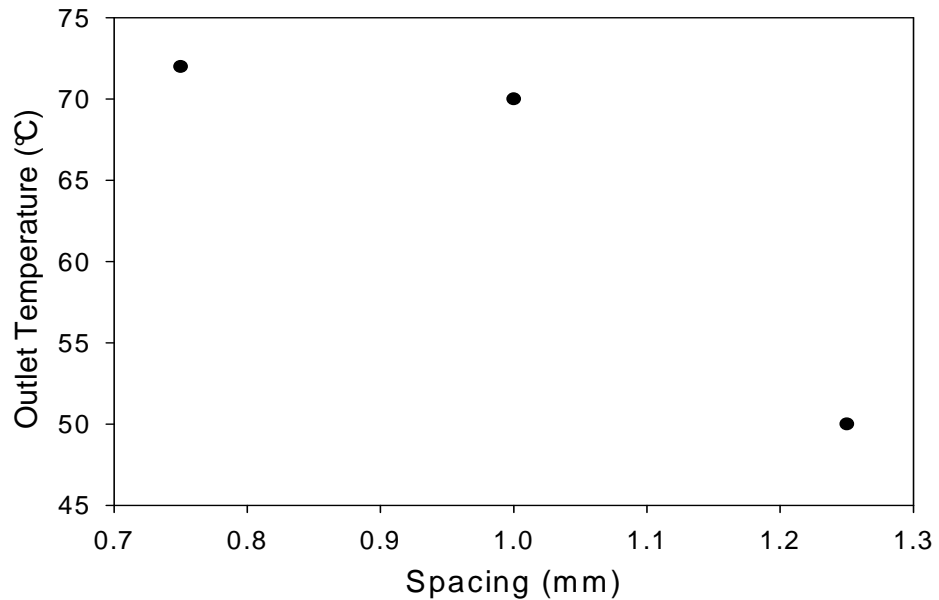


Figure 24. Temperature with Spacing at 100 psig, 1210 RPM and 180 seconds Time

However, the temperature requirements have been achieved so further reduction was not deemed necessary. This table is at constant feed pressure of 100 psig, 1209 rpm and 180 seconds holdup time. After 180 seconds, the rubber stop cork was removed and the mass was allowed to leave to the environment. The mass was observed to be hot and moist, and dried quickly when open in the air. If we summarize the results, higher hold up time and lower spacing enhances outlet temperature. In the next attempt, the effect of rpm on temperature rise is evaluated (table 9). We see at 100 psig feed pressure, 0.75 mm spacing, and 180 seconds hold up time, that the temperature rises linearly

Table 9. Temperature with RPM change at Constant Pressure, Time and Spacing

Feed	Feed Pressure	Spacing	Hold up Time	rpm	Outlet temperature
	psig	mm	seconds		°C
Red Potato	100	0.75	180	913	55
				1209	72
				1504	104

The objective is to define the conditions where a temperature of 120°C is achieved for the effluent mass. This temperature is sufficient to sanitize the waste and operation at higher conditions supplies additional energy with the only benefit being increased water evaporation rate. The ‘cost’ for the additional temperature depends on the equipment and utility costs. The operation conditions must be based on an optimization of these operational (energy cost) and capital (equipment wear) related factors.

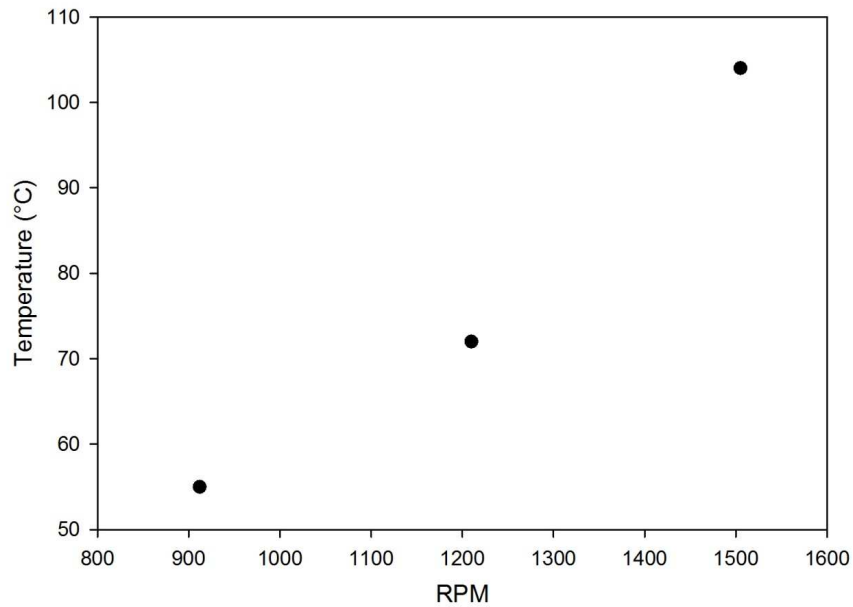


Figure 25. Temperature with RPM Change at 100 psig, 180 seconds Holdup time and 0.75 mm Spacing

5.3 RESULT OF LONGER OPERATION

In order to reach maximum possible temperature, simulant (boiled red potato and mashed) was fed into the reactor. The reactor pressure was set at 70 psig and inverter reading of 60HZ. This reading from inverter is equivalent to 1790 rpm measured by the non contact ledger tachometer. The smallest gap spacing of 0.75mm was maintained throughout the operation. The stop cork was held on the outlet and kept close for about 480 seconds (8 minutes). Due to high temperature rise, the cork was not possible to hold more than 8 minutes. A continuous 120 seconds (2 minutes) was observed after the 8 minutes of operation, when the cork was removed. More vapors could be observed if the reactor was allowed to run more than 2 minutes. To minimize risk of any accident, the motor was stopped after 10 minutes of operation. Figure 26 shows the burnt mashed potatoes cling to the surface of the cone after dissembled the setup.



Figure 26. Burnt Mashed Potato Layer over the Cone Surface

Though we found a temperature reading of 95°C only at end of 8 minutes, we observed a significant amount of vapor flow for about 2 minutes. The temperature reading for different hold up time for this experiment is given in table 10. The temperature rise is lower in the outlet product is due to vaporization of the water containing in the potato and a low pressure operation. Due to unavailability of the necessary amount of pressure accessories, the experiment was run at low pressure (70 psig). While longer higher hold up time enhanced the viscous heating in the simulant (mashed potatoes), the low pressure helped vaporize a portion of water from it. The temperature rise in table 9 was low enough in comparison to the temperature data mentioned in previous tables. Because in previous operations, heat produced by viscous heating was only used to increase the temperature of the simulant material. But for experimentation for longer hold time at a low pressure, the water containing in the simulant absorbed the latent heat of vaporization

and created the vapor. This resulted into a low temperature rise in the paste exiting the outlet. Since most of the heat produced by viscous heating was utilized to produce vapor and the simulant paste absorbed lower amount of heat in contrast to previous operations at 100 psig.

Table 10. Temperature Time at 70 Psig, 0.75 mm Spacing and 1790 RPM

Feed	Feed Pressure	Spacing	rpm	Holdup Time	Outlet Temperature
	psig	mm		seconds	°C
Red Potato	70	0.75	1790	60	54
				120	61
				180	69
				240	78
				480	95

The product from the reactor after 8 minutes run was almost dry. When allowed to leave the rector, almost dried paste became dried over the surface of the shell (Figure 27) within 5 seconds. When the reactor was disassembled, a remnant paste was burnt and brown in color. We observed small amount of dried potato chips as product. When rubbed by hands, the chip like product was broken into parts.



Figure 27. The Cone and the Shell after 8 minutes (480 seconds) Run

5.4 PARASITE DESTRUCTION

The kill rate for parasite eggs is shown in table 6. Although the rpm in table 11 is according to the reading correlated with power input to the inverter, the speed might be lower because of the presence of a considerable amount of baboon hair in the sample, which is typical for baboon feces due to their grooming habits. This affects the ability of the outlet product to achieve high temperature.

Table 11. Percentage Parasite Egg Destruction with Variable Settings

RPM	Spacing	Temperature	Pretreatment	Post Treatment	Percentage kill
	mm	°C	EPG*	EPG*	%
913	1.20	42	107.1	7.7	93
913	0.75	51	166.5	1.7	99
1800	0.75	86	58.0	2.8	95

**Trichuris trichiura* eggs per gram of baboon feces

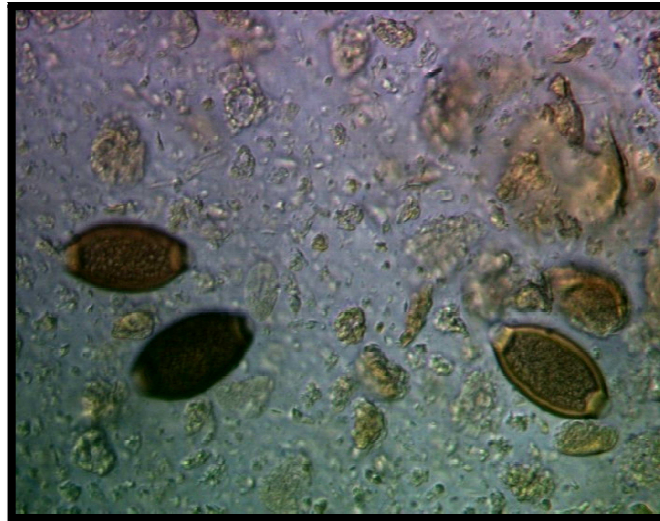


Figure 28. Photomicrographs of *Trichuris trichiura* Eggs from Helium before Being Processed through the Extruder (400 x Magnifications)

A destruction approaching 99% was achieved for the *Trichuris trichiura* eggs. The temperature achieved for smallest spacing (0.75 mm) and the highest rpm setting (1800 calculated, but

believed to be lower in actuality.) was not as high as the red potato samples. However, the kill rate of *Trichuris trichiura* was high, indicating destruction from shear stress alone. Figure 28 and 29 show photomicrographs for the destruction of the *Trichuris trichiura*. The pressure used in the study of table 6 is not known since a manual, variable pressure was applied due to the lack of available building gas in the BSL-2 laboratory. Repeated experiments will have an equipment modification to allow for controlled pressure. Figure 28 shows some *Trichuris trichiura* eggs present in a processed sample of Baboon feces. The irregular-shaped large cellular materials are most likely partially digested plant material. As can be seen, there are 4 eggs of *Trichuris trichiura*. They are football to lemon shaped, stained dark brown with a smooth shell.

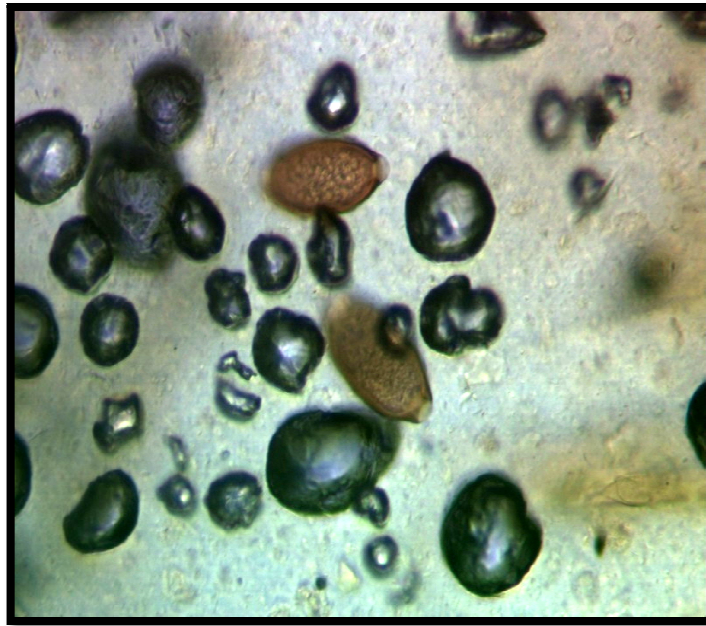


Figure 29. Photomicrographs of *Trichuris trichiura* Eggs from Helium after Being Processed through the Extruder (400 x Magnifications)

Figure 29 shows that air bubbles because of processing through the device accompany the destruction of *Trichuris trichiura*. As can be seen, all the dark round structures are air bubbles in the 400x magnification photomicrograph notice the fine particulate matter that makes the

background appear cloudy. In the bottom (post-treatment through the extruder) notice the somewhat irregular round structures. These structures appear to be find grains of sand broken down small enough by the extruder that make them small enough to disperse in the flotation solution. Air enters through the hole (feed inlet) while the plunger pushes the feed inside the chamber. Under high rotation, air bubbles form and mix with the feed. As air is not highly viscous, there is a potentially negative effect on the high viscosity desired of the mixture. The reduced viscosity due to the presence of air may be a contributing factor in the lower temperatures observed with baboon feces.

5.5 EXPERIMENTS WITH ADDITIVES

Experiment was performed with a mixture of sweet potatoes, grass and toilet paper. The potatoes were boiled for one hour. Grass and Toilet paper were cut into small pieces by a scissor. A mixture was produced by hand and feed into the reactor. The mixture was not completely uniform. The experimental setting was maintain at 100 psig feed pressure, 1800 rpm and 1.25mm gap spacing. The gap spacing was kept higher for these operations because of the clogging nature of the mixture. Past experiment with smaller gap spacing such as 0.75mm and 1 mm, clogged the inlet and charging feed continuously was interrupted.



Figure 30. Temperature Reading for Experimentation with Grass, Sweet Potato & Toilet Paper

The operation was carried out for 240 seconds keeping the outlet close with the black rubber cork. A final temperature of 145.6 °C was recorded. The readout is shown in figure 30. The reason for rising of high temperature is because of adding grass and toilet paper. The cellulose in grass and toilet paper contributed significantly to keep the viscosity of the feed material constant after sometimes starting the operation. As viscous heating phenomenon is responsible to decrease the viscosity of the feed material, the added grass helped increase or keep constant the overall viscosity of the mixture. The reason for choosing grass in this experiment was that, in rural application, grass should be available in the spot and can be used either free or at nominal cost. In addition, a practically feasible solution always was a consideration while designing and operating the reactor. The product looked like chicken cecale (Figure 31). The funding provider, Bill & Melinda Gates Foundation had a requirement that no chemical additive could be used to process feces. We also believe that saw dust and any other sorts of paper additive might be helpful to increase the viscosity of the feed material. Further rheology experiments using potential additives are necessary to select materials to increase shear.



Figure 31. Product of Experimentation with Grass, Toilet Paper & Sweet Potato

5.6 PEANUT BUTTER EXPERIMENT

Peanut butter was fed to the reactor to observe temperature rise with a low viscosity paste. The efficacy of viscous heating could be understood for low viscosity human feces such as diarrheal

stool. Peanut butter was bought from local Walmart. The butter was fed to the reactor at an inverter reading of 60 Hz, an equivalent rpm reading of 1790. The experiments were performed by manual pressure due to shortage of air pressure in the laboratory. Three different spacing were set to gather data for outlet temperature. As can be seen, from Table 12, as the spacing value decreases, the outlet temperature increases. Following is the experimental result with peanut butter.

Table 12. Experimental Result for Peanut Butter Run

Feed Pressure	Spacing	Inverter Reading	rpm	Holdup Time	Outlet Temperature
psig	mm	Hz		seconds	°C
Manual	1.25	60	1790	290	76
Manual	1.00	60	1790	280	113
Manual	0.75	60	1790	280	123

Peanut butter has a low viscosity in comparison to the viscosity of potato/human feces. The butter was melted approximately at 90 seconds of operation due to the heat produced by viscous heating effect of the primarily charged butter and created a diarrheal stool like liquid in the inlet even at low temperature. Heat was transmitted to the upper surface and other connected parts of the reactor. Clearly the findings indicate that the temperate with the highest setting of the reactor (spacing=0.75mm and rpm=1790), the temperature at outlet is 123°C. From table 7, for this similar setting temperature reading of outlet at 260 seconds is 190°C for potato, a comparatively higher value because of higher viscosity of fed material.

5.7 REACTOR PROFILE

Vegetable dye solution was injected to determine the reactor profile. The plunger was removed and mashed potatoes were fed by the operator in the gap of the core and shell (figure 32).

Vegetable dye solution was passed through the reactor inlet into the mashed potatoes with a syringe. The cone was run for 15 seconds and stopped; keeping the inlet closed using a thick cotton pad. The reactor body was carefully dissembled for each run. Photographs determined the nature of spreading.

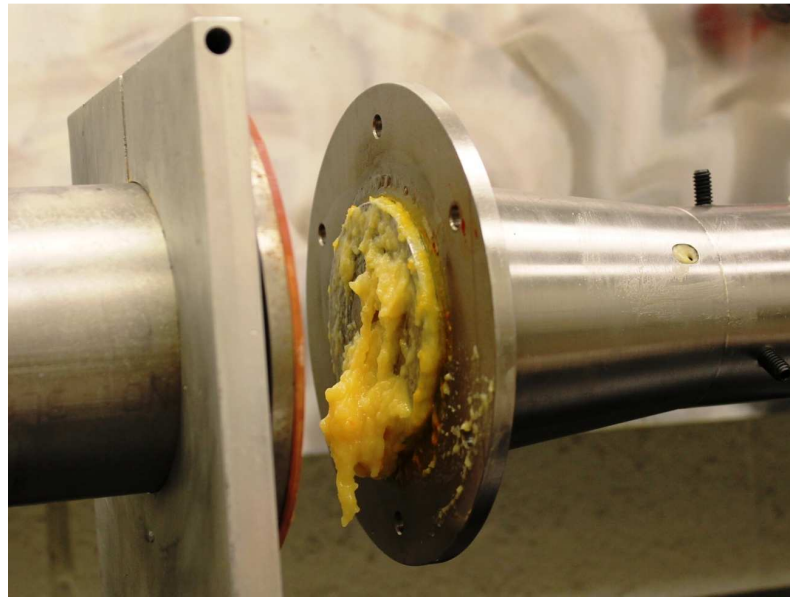


Figure 32. Charging Mashed Potatoes Manually by Operator

Figure 33 displays the reactor profile. Simulant spread in a sinusoidal or parabolic curve indicating an infinite number of CSTRs (Continuous Stirred Tank Reactors) creating a unique plug flow profile since little color dispersed in the axial direction.



Figure 33. Vegetable Dye Passing through the Reactor to Determine Flow Pattern

We can determine the inlet and outlet tangential velocity using the radius of the cone in the inlet and outlet and angular velocity. From figure 34, the inlet radius r_i and outlet radius r_o is 0.999 and 1.4625 inch respectively. Therefore for a certain angular speed ω , the inlet outlet tangential velocity equation would be,

$$(V_i)_t = \omega r_i \quad (10)$$

$$(V_o)_t = \omega r_o \quad (11)$$

Dividing equation 10 by equation 11 we have,

$$\frac{(V_i)_t}{(V_o)_t} = \frac{r_i}{r_o}$$

$$\frac{(V_i)_t}{(V_o)_t} = \frac{1.4625}{0.999} = 1.464 \cong 1.5$$

$$(V_i)_t = 1.5(V_o)_t$$

So inlet tangential velocity is 1.5 times of outlet tangential velocity.

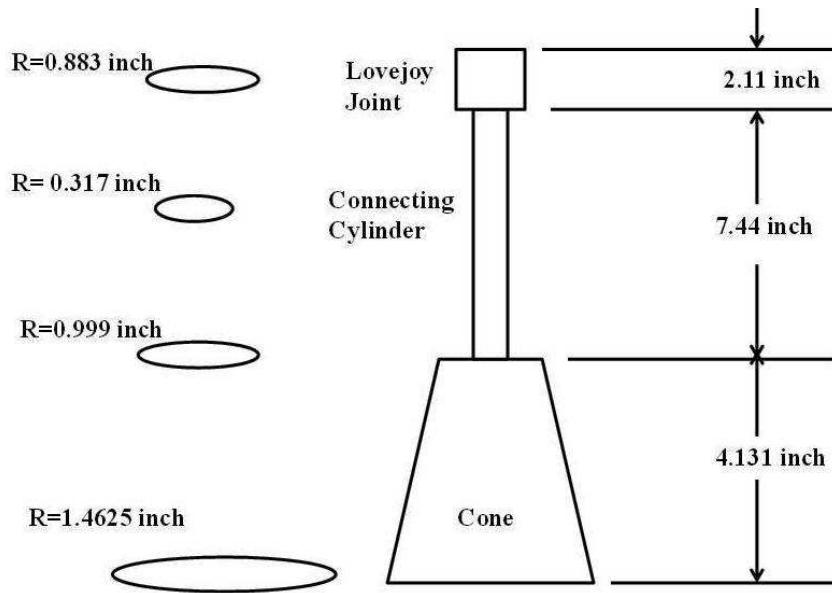


Figure 34. Dimension of the Cone and Other Rotating Parts

We can also get an idea of inlet and outlet axial velocity relationship using the equation of continuity.

$$(V_i)_a A_i = (V_o)_a A_o$$

$$\frac{(V_i)_a}{(V_o)_a} = \frac{A_o}{A_i} \quad (12)$$

$$A_i = \pi \{ (r_o)_{inlet}^2 - (r_i)_{inlet}^2 \} \quad (13)$$

$$A_o = \pi \{ (r_o)_{outlet}^2 - (r_i)_{outlet}^2 \} \quad (14)$$

For both cases in the inlet and outlet the outer radius is summation of inner radius and spacing

So we have,

$$r_o = r_i + s$$

$$(r_o)^2 = (r_i + s)^2 = r_i^2 + 2r_i s + s^2$$

$$\text{So } (r_o)^2 - (r_i)^2 = 2r_i s + s^2$$

Putting in equation 13 and 14, we have

$$A_i = \pi \{ 2(r_i)_{inlet} s + s^2 \}$$

$$A_o = \pi \{ 2(r_i)_{outlet} s + s^2 \}$$

Equation ... becomes,

$$\frac{(V_i)_a}{(V_o)_a} = \frac{A_o}{A_i} = \frac{2(r_i)_{outlet} s + s^2}{2(r_i)_{inlet} s + s^2}$$

$$\frac{(V_i)_a}{(V_o)_a} = \frac{(r_i)_{outlet} + \frac{s}{2}}{(r_i)_{inlet} + \frac{s}{2}} \quad (15)$$

Since, $(r_i)_{inlet} > (r_i)_{outlet}$

$$\frac{(V_i)_a}{(V_o)_a} < 1$$

$$(V_i)_a < (V_o)_a$$

Putting the values of $(r_i)_{\text{outlet}}$ and $(r_i)_{\text{inlet}}$ from figure 34 in equation 15 at spacing 0.75 , $s=0.75\text{mm}$
 $=0.03$ inch ,we have

$$\frac{(V_i)_a}{(V_o)_a} = \frac{(r_i)_{\text{outlet}} + \frac{s}{2}}{(r_i)_{\text{inlet}} + \frac{s}{2}}$$

$$\frac{(V_i)_a}{(V_o)_a} = \frac{0.999 + 0.03}{1.4625 + 0.03} = 0.69 \quad (16)$$

$$(V_i)_a = 0.69 (V_o)_a \quad (17)$$

5.8 SHEAR STRESS ANALYSIS

The equation of shear rate is

$$\gamma = \frac{v}{h}$$

Where γ = Shear rate

v = velocity of the moving plane

h = Distance between two parallel planes=Spacing

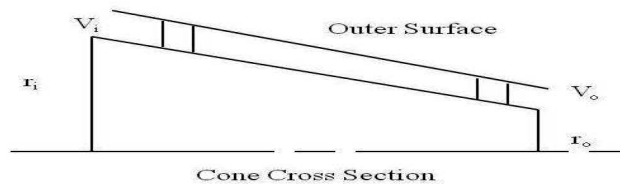


Figure 35. Shear Rate Analysis

5.8.1 COMPARISON OF INLET AND OUTLET TANGENTIAL SHEAR RATE

Inlet tangential shear rate = $(\gamma_i)_t$

Outlet tangential shear rate = $(\gamma_o)_t$

Inlet tangential velocity, $(V_i)_t = \omega r_i$

$$\text{Inlet tangential shear rate, } (\gamma_i)_t = \frac{(V_i)_t}{h} = \frac{\omega r_i}{h} \quad (18)$$

Outlet velocity, $(V_o)_t = \omega r_o$

$$\text{Outlet shear rate, } (\gamma_o)_t = \frac{(V_o)_t}{h} = \frac{\omega r_o}{h} \quad (19)$$

Dividing equation 18 by equation 19, we have

$$\frac{(\gamma_i)_t}{(\gamma_o)_t} = \frac{(V_i)_t}{(V_o)_t} = \frac{r_i}{r_o}$$

$$\frac{(\gamma_i)_t}{(\gamma_o)_t} = \frac{1.4625}{0.999} = 1.464 \cong 1.5$$

$$(\gamma_i)_t = 1.5(\gamma_o)_t$$

So inlet tangential shear rate is 1.5 times higher than the outlet tangential shear rate. Tangential shear rate decreases along the length of the reactor.

5.8.2 COMPARISON OF INLET AND OUTLET AXIAL SHEAR RATE

Inlet axial shear rate = $(\gamma_i)_a$

Outlet axial shear rate = $(\gamma_o)_a$

Inlet axial velocity = $(V_i)_a$

$$\text{Inlet axial rate, } (\gamma_i)_a = \frac{(V_i)_a}{h} \quad (20)$$

Outlet axial velocity = $(V_o)_t$

$$\text{Outlet axial shear rate, } (\gamma_o)_a = \frac{(V_o)_a}{h} \quad (21)$$

Dividing equation 20 by equation 21, we have

$$\frac{(\gamma_i)_a}{(\gamma_o)_a} = \frac{(V_i)_a}{(V_o)_a} = 0.69$$

$$(\gamma_i)_a = 0.69 (\gamma_o)_a$$

5.9 VOLUME OF THE REACTOR

The volume of the reactor was determined feeding water with a syringe in between the gap of shell wall and the core. The outlet and other gaps were covered with black electrical tape. Some molten wax from a flaming candle was added to the contact area of the bearing (figure 36). Any gap in these areas was completely sealed so that no water comes out of the system. A 20 ml cylinder was filled with water and with help of syringe needle water was passed through the gap and filled completely. The initial and final volume reading were recorded and volume inside the reactor determined for the gap spacing of 0.75mm. The volume of the reactor was found to 15ml for this spacing setting. Also the reactor was filled with water using tape without putting wax to determine if there is any leak in the system. As can be seen from figure 37, water is leaking out of the system. The reactor setup was kept leaned over a wall in the laboratory for few minutes. Water was coming out similar to drop wise condensation phenomenon. So the system not completely air tight.



Figure 36. Determination of Volume inside the Reactor

We conclude that the pressure applied in the feed is not completely constant inside the reactor and should be less than the inlet pressure at outlet. With the current geometry and setup of the reactor, it is not possible to determine the outlet pressure. A separate gauge might be set in the outlet to determine the outlet pressure.



Figure 37. Water Leak from the Reactor when Charged

5.10 SECOND PROTOTYPE

The second prototype was designed based on the working mechanism of first one (Figure 36). But there are few exceptions such as the second one has only fixed spacing of 1mm. The feed material is charged on the top (vertically) of the cylinder and the black plunger is used to push the material inside it. The AC motor can rotate the shaft from 0 to 1200 rpm at a variable speed. The motor installed here was bought from general hardware store. No pressure controlling gauge was installed in this unit to keep the design similar to reality. Around the outlet the yellow color polymer material is to instantly remove the product immediately from the outlet.

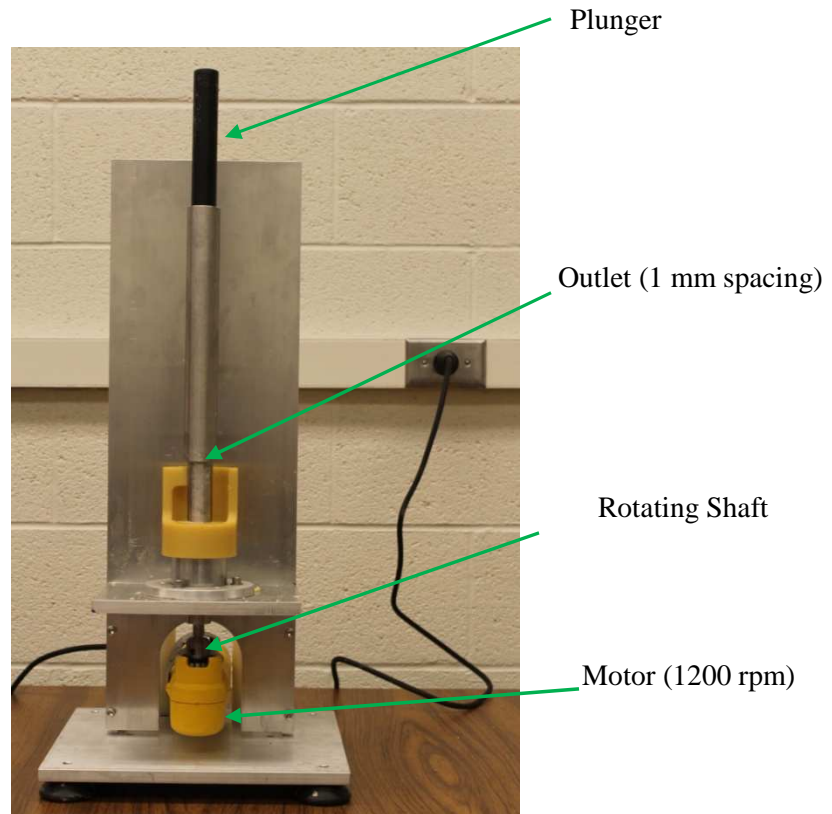


Figure 38. Design Improvement of the Viscous Heating Mechanism (Second Unit)

The main difficulty we faced to experiment with the this reactor was the outlet flow control . There was not enough outlet controlling provison to prevent the flow during hold up time. Coiled paper towel was held tightly on the outlet duration the operation. The result is shown in table 13.

Table 13. Outlet Temperature Reading for Different Holdup Time

Potato	Feed Pressure	RPM	Spacing	Holdup time	Outlet Temperature
			mm	seconds	°C
Red	Manual	1000	1	270	47
Red	Manual	1000	1	180	41

CHAPTER VI

ENERGY BALANCE

To start with an energy balance, first we need to determine the energy input and energy output of the system. Electrical Energy is used to run the Lincoln Electric NEMA Design B Motor. In addition, the work done by the plunger to push (in general at 100 psig) the mass inside the system is another energy input into the system. The rotational (kinetic energy) the motor shaft is used to rotate the cone, tapered bottom bearing, love joints, star connector and other rotating parts attached to the cone. A portion of the motor energy is used to produce heat in the input mass (either simulant or human feces). This heat is observed as the temperature rise of the final product from the reactor. A third portion of energy is dissipated in form of heat due to friction of metallic joints of different parts of the system and sounds. So if we balance different forms of energy input and output, energy balance equation becomes

Input= Output

Work done by the plunger +Work done by the motor = Kinetic Energy of the Shaft + Heat gain by the product + Heat transfer by the product +System Loss

$$\text{Or, } W_p + W_m = E_k + Q_p + H_t + E_l \quad (22)$$

Where

W_p = Work done by the plunger

W_m = Work done by the motor under no load condition

E_k = Kinetic Energy of the Shaft

Q_p = Heat gain by the product

H_t = Heat transfer to the environment

E_l = System Loss

We would perform an energy balance for a 240 seconds (4 minutes) run at 100 psig, 1800 rpm and 0.75mm gap spacing.

6.1 Work Done by the Plunger, W_p

The work done by the plunger is equal to the product of pressure applied to push the mass inside the system and the volume of the mass. The volume of the mass would be equal to the volume to the volume of the reactor. This amount of volume was kept inside the system during the operating periods (hold up time). As we ran most of our operation and 100 psig, the calculation of work is given below based on this pressure. Also here the calculation is give for 0.75mm spacing. For other operating pressure, the calculation should be corrected accordingly.

Pressure, $P = 100 \text{ psig} = (100 + 14.7) \text{ psia}$

$$= 114.7 \text{ psia}$$

$$= 114.7 * 6894.757 \text{ N/m}^2$$

$$= 790828.66 \text{ N/m}^2$$

Volume Reduction, $\Delta V = \text{Volume of gap in between the shell and the core}$

$$= 15 \text{ ml (For 0.75mm spacing gap)}$$

$$= 15 \text{ cm}^3$$

$$= 15 \times 10^{-6} \text{ m}^3$$

So, Work done by the plunger, $W_p = P \Delta V$

$$= (790828.66 \text{ N/m}^2) 15 \times 10^{-6} \text{ m}^3$$

$$= 11.86 \text{ Joule}$$

$$= 0.01 \text{ KJ}$$

6.2 Work Done by the Motor, W_m

A wattmeter from was installed in the power supply line of the motor of the reactor to account energy balance. Mashed potatoes was charged in the reactor and experiment was performed for 100 psig feed pressure, 0.75 mm gap spacing and 1800 rpm setting for a hold up time for 260 seconds (time to achieve 190°C per table 3) for two different condition-without charging any feed into the reactor and with charging feed. For both cases, power consumption was recorded every 10 seconds. A plot of instantaneous power versus time was obtained for both no load and load conditions (Figure 39). Energy input to the feed (mashed potato) was calculated, subtracting the two values.

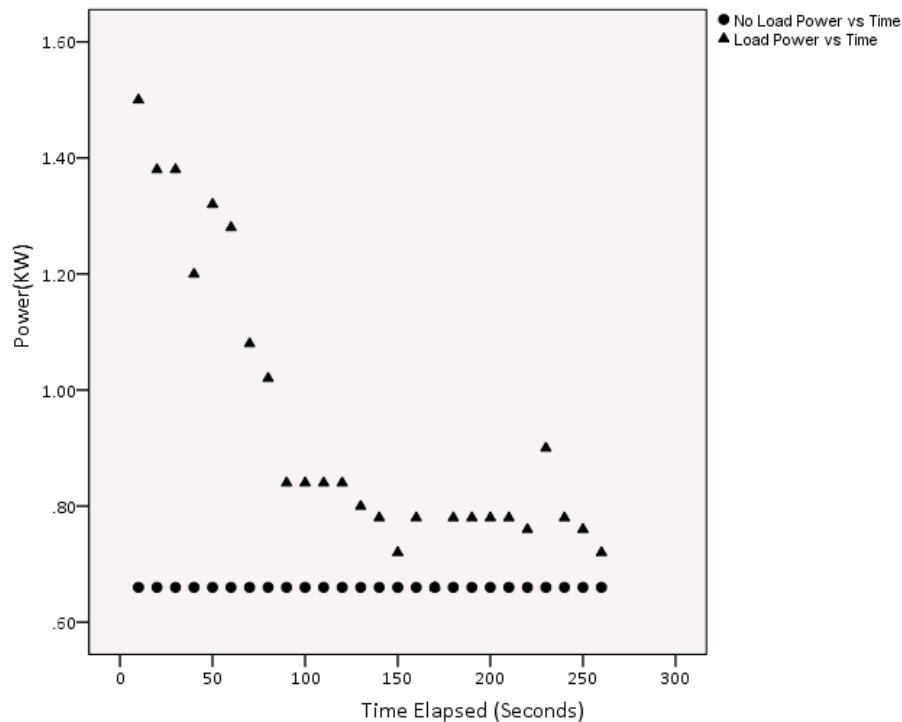


Figure 39. Power versus Time for No Load and Load Conditions at 100 psig, 0.75mm spacing and 1800 rpm

The area under the curve of power versus time (Figure 39) gives the total energy consumed. For a 260 second run, the energy with load totaled 243 KJ, while that without load was 172 KJ; for a difference of 71 KJ.

Work done by the motor = Energy under no load condition

$$=171 \text{ KJ}$$

The heat transfer to the environment through the metallic surface and heat retain by the product is the difference of energy under load and no load condition.

So, $Q_p + H_t = 243 - 171 = 72 \text{ KJ}$

$$Q_p + H_t = 72 \text{ KJ} \tag{23}$$

Most of the energy input to the simulant occurs in the first 90 seconds and then a near steady state is achieved. Most of the temperature rise occurs in this first region and then temperature increases gradually, nearly at steady state.

6.3 Kinetic Energy of the Shaft, E_k

We would calculate the kinetic energy by the following energy equating of a rotating object,

$$E_k = \frac{1}{2} I \omega^2 \tag{24}$$

Where

$I =$ Moment of inertia $= \int r^2 dm$

$\omega =$ angular velocity (radian/second) $= 2 * \pi * n$

RPM recorded from Tachometer $= 1800$

$n = 1800 / 60$ rotation per seconds $= 30$

$\omega = 2 * \pi * 30 = 188.5 \text{ rad/sec}$

Now we need to calculate the moment of inertia for different parts of the rotating body. The geometry was measured by slide calipers (Figure...) The rotating setup consists of three main

parts such as the cone, the connecting cylinder and the love joint. Though the lovejoy coupling joint has a plastic star shaped connector in between, for calculation simplicity we assumed it to be solid. Also due to very small weight, the weight nut and black rubber seal were also neglected in this calculation.

The total moment of inertial I would be equal to the moment of inertial of the lovejoy coupling joint, connecting cylinder and the cone.

$$\text{So } I = I_C + I_{CC} + I_{LJ}$$

Where I_C = Moment of inertia of cone

I_{CC} = Moment of inertia of connecting cylinder

I_{LJ} = Moment of inertia of lovejoy coupling joint

For calculating moment of inertia we divide the cone shown in figure 34 in three different parts

6.3.1 Moment of inertia of cone, I_C

The cone part (hatched) is shown in figure 34. The dimensions were calculated using geometric knowledge. We borrowed following calculations from Beer & Johnston (1990). We choose the differential element of mass

$$r = a \frac{x}{h}$$

Where

a = radius of the cone

h = Height of the cone

$$dm = \rho \pi r^2 dx = \rho \pi \frac{a^2}{h^2} x^2 dx$$

For a thin disk, we compute the mass moment of inertia of the differential element with respect to the rotating axis

$$dI_C = \frac{1}{2} r^2 dm$$

$$= \frac{1}{2} \left(a \frac{x}{h} \right)^2 \left(\rho \pi \frac{a^2}{h^2} x^2 dx \right)$$

$$= \frac{1}{2} \rho \pi \frac{a^4}{h^4} x^4 dx$$

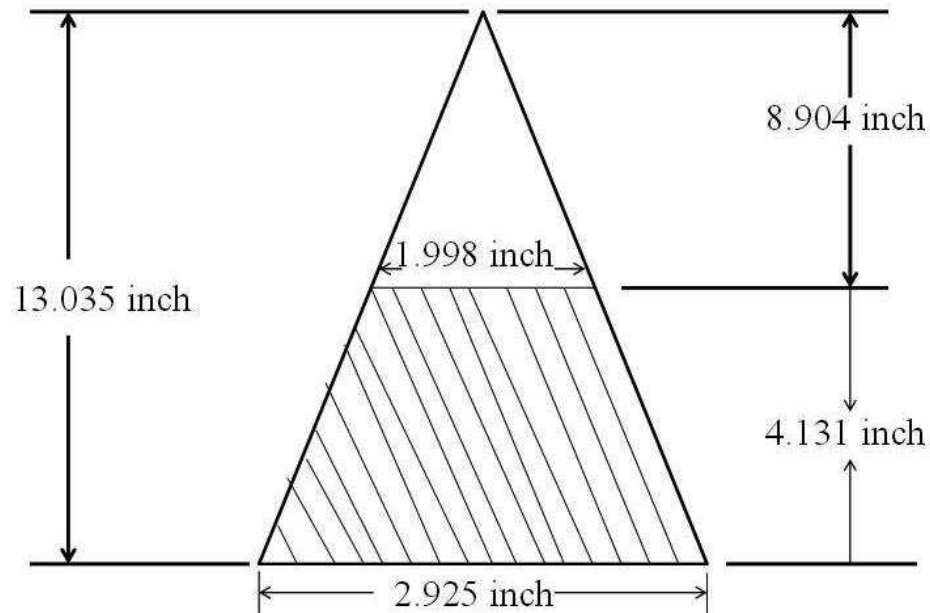


Figure 40: Cone Geometry

$$\rho = \rho_{\text{steel}} = 8.027 \text{ gm/cm}^3 = 8027 \text{ kg/m}^3 \text{ (Murray 1997)}$$

$$a = 1.4625 \text{ inch} = 0.0371 \text{ m}$$

$$h = 13.035 \text{ inch} = 0.3311 \text{ m}$$

Integrating from $x=8.904$ inch to $x=13.035$ inch, we obtain

$$\mathbf{I}_C = \int dI_x$$

$$= \int_{8.904 \text{ inch}}^{13.035 \text{ inch}} \frac{1}{2} \rho \pi \frac{a^4}{h^4} x^4 dx$$

$$= \int_{0.2262 \text{ meter}}^{0.3311 \text{ meter}} \frac{1}{2} \rho \pi \frac{a^4}{h^4} x^4 dx$$

$$= \frac{1}{10} \rho \pi \frac{a^4}{h^4} [x^5]_{0.2262}^{0.3311}$$

$$= \frac{1}{10} * \rho \pi \frac{a^4}{h^4} * [0.3311^5 - 0.2262^5]$$

$$= \frac{1}{10} * (7850 \text{ kg/m}^3) * (3.1416) * \frac{0.0371^4}{0.3311^4} * [0.3311^5 - 0.2097^5] \text{ m}^5$$

$$= 0.0014 \text{ kgm}^2$$

6.3.2 Moment of inertia of Connecting Cylinder, I_{CC}

From Beer & Johnston (1990), the equation for the moment of inertia for a cylindrical rotation body is as follows

$$I_{CC} = \frac{1}{2} ma^2$$

Where m = mass of the cylinder

a = radius of the cylinder

Volume of the cylinder, $V = \pi a^2 h$

So mass, $m = \rho V$

$$= \rho \pi a^2 h$$

$$I_{CC} = \frac{1}{2} \rho \pi a^4 h \quad (25)$$

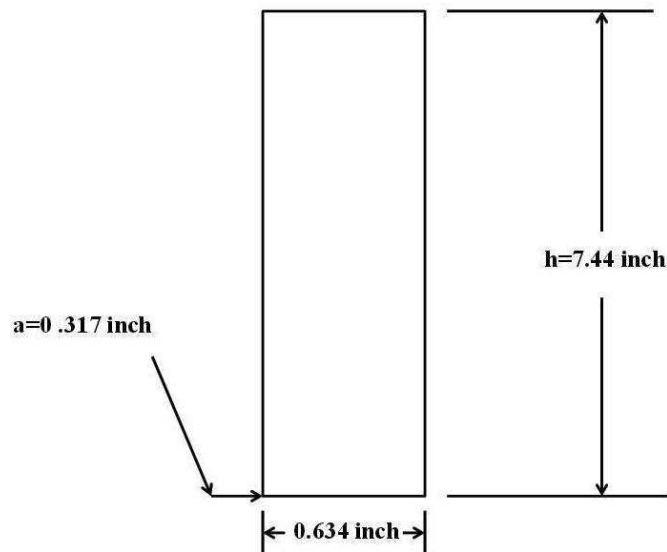


Figure 41. Geometry of Connecting Cylinder

Here $\rho = 7850 \text{ kg/m}^3$

$a = 0.317 \text{ inch} = 0.0081 \text{ m}$

$h = 7.44 \text{ inch} = 0.189 \text{ m}$

$$I_{CC} = \frac{1}{2} \rho \pi a^4 h$$

$$= \frac{1}{2} * 7850 \text{ kg/m}^3 * 3.1416 * (0.0081\text{m})^4 * (0.189\text{m})$$

$$= 0.00001 \text{ kgm}^2$$

6.3.3 Moment of Inertia of Lovejoy Coupling Joint, I_{LJ}

As the lovejoy coupling joint is cylindrical in shape, we can use equation similar to equation 25

$$\text{So the moment of inertial, } I_{LJ} = \frac{1}{2} \rho \pi a^4 h$$

Here radius, $a = 0.883 \text{ inch} = 0.0224 \text{ m}$

Height, $h = 2.11 \text{ inch} = 0.0536 \text{ m}$

$$I_{LJ} = \frac{1}{2} \rho \pi a^4 h$$

$$= \frac{1}{2} * 7850 \text{ kg/m}^3 * 3.1416 * (0.0224\text{m})^4 * (0.0536\text{m})$$

$$= 0.0002 \text{ kgm}^2$$

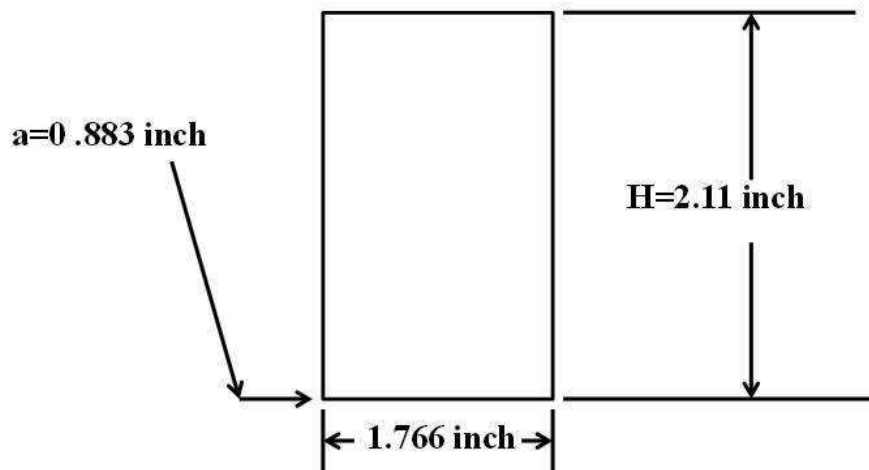


Figure 42. Geometry of Lovejoy Coupling Joint

$$\text{So total moment of inertia, } I = I_C + I_{CC} + I_{LJ}$$

$$= (0.0014 + 0.00001 + 0.0002) \text{ kgm}^2$$

$$= 0.00161 \text{ kgm}^2$$

Recall equation 24.

$$E_k = \frac{1}{2} I \omega^2$$

$$\begin{aligned}
&= \frac{1}{2} * (0.00161 \text{ kgm}^2) * (188.5 \text{ rad/sec})^2 \\
&= 28.60 \text{ J} \\
&= \mathbf{0.03 \text{ KJ}}
\end{aligned}$$

6.4 HEAT GAIN BY THE PRODUCT (POTATO), Q_p

Specific of potato, $C_{\text{potato}} = 3.43 \text{ KJ/Kg.K}$ (www.engineeringtoolbox.com/specific-heat-capacity-food-d_295.html)

Room Temperature, $T_0 = 25^\circ\text{C}$

Temperature rise, $T_{\text{final}} = 190^\circ\text{C}$

Time required to reach 190°C , $t = 4 \text{ min}$

$$= 240 \text{ seconds}$$

Density of potatoes (red), $\rho_{\text{potato}} = 1.0796 \text{ gram/cm}^3$

Volume of gap in between the shell and the core, $V = 15 \text{ ml}$ (For 0.75 mm spacing gap)

$$= 15 \text{ cm}^3$$

Mass of potato processed in the reactor, $m_p = \rho_p * V$

$$= (1.0796 \text{ gram/cm}^3) * (15 \text{ cm}^3)$$

$$= 16.194 \text{ gram}$$

$$= 0.016194 \text{ Kg}$$

Heat produced in 4 minutes, $Q_p = Q_{\text{potato}}$

$$= m_p * C_{\text{potato}} * (T_{\text{final}} - T_0)$$

$$= (0.016194\text{Kg}) * (3.43 \frac{\text{KJ}}{\text{Kg.K}}) * (190-25) \text{ K}$$

$$= 9.16 \text{ KJ}$$

6.5 FINAL ENERGY BALANCE & SYSTEM EFFICIENCY

Recall equation 22

$$W_p + W_m = E_k + Q_p + H_t + E_l$$

Where

W_p = Work done by the plunger = 0.01 KJ (Negligible)

W_m = Work done by the motor = 171 KJ

E_k = Kinetic Energy of the Shaft = 0.03 KJ (Negligible)

Q_p = Heat gain by the product = 9.16 KJ

H_t = Heat transfer to the environment by the system = (71 - 9.16) KJ

$$= 61.84 \text{ KJ}$$

Neglecting work done by plunger and kinetic energy of the shaft, we have

$$W_m = Q_p + H_t + E_l$$

System Loss, $E_l = W_m - (Q_p + H_t)$

$$= (172 - 72) \text{ KJ}$$

$$= 100 \text{ KJ}$$

If the metallic surface is coated with heat insulator, the heat transfer term would be zero. So under insulated condition, $H_i=0\text{KJ}$ and a higher temperature rise is expected. At this condition, the system efficiency would be as follows,

$$\begin{aligned} \text{System Efficiency, } \eta &= \frac{\text{Heat gain by the product} + \text{Heat Transfer to the Environment}}{\text{Work done by the motor under load condition}} \\ &= \frac{72}{243} \\ &= 29.6\% \end{aligned}$$

Some energy is retained by the mass, but most is conducted out through the metal shell and core. If the experiment stopped at 90 seconds 48% of the energy input would go to the mass. After viscosity of the simulant has been reduced due to temperature increase less energy is required to maintain the same rpm. With lower viscosity, less energy goes to viscous heating. The longer the system runs at steady state, the lower the percentage of total energy goes into the simulant. By the end of the full 260 second run the total fraction of energy that was input into the simulant was 29%. This percentage would continue to drop with increasing run time. Clearly, if viscous heating is the goal then the device should be stopped at 90 seconds or configured to operate with steady state flow rate of simulant. For a given rpm and geometry the simulant flow rate can be established for a fixed percentage power input between 29% and 48%. However, if a specific temperature is required then a singular efficiency will result.

CHAPTER VII

CONCLUSION

CFD studies showed the temperature gradient in the reactor depends significantly on the angular velocity, inlet velocity, clearance, and length. Simulations agreed with the experimental data. Experimentation confirmed that viscous heating by extrusion may be effective in decontaminating fecal wastes. For each experiment, fixing two variables from among rpm, holdup time, and gap spacing allowed one variable to be compared with the resulting temperature change. Temperature was observed to increase with decreasing space, increasing rpm, and increasing contact time. Shear force and viscous heat are sufficient to kill diseases causing parasites. The maximum temperature achieved was 190°C within 3-4 minutes with mashed red potatoes.

The hot moist simulant from the reactor dried in open air within 10-15 minutes. In contact with the reactor surface, a thin film of moist potato was turned into crunchy chips. Destruction of *Trichuris Trichiura* eggs were observed despite elevated temperatures not being achieved, indicating sheer stress alone as an effective mechanism.

Since extrusion is proven, application of the technology is likely to have a place for specific situations. Combination with other treatment technologies may be appropriate. A primary challenge to dewater the effluent is being addressed. Optimization of the operating conditions can achieve sufficient temperature while minimizing equipment wear and energy input.

A significant factor is the requirement of high viscosity to generate heat. For cases where people have diarrhea, where urine is not separated nor when water is added by rain or other means, this technology requires modification to increase the feed viscosity. Possibilities include the addition of paper or biomass wastes or design that includes recycle of some of the drier solid waste. By balancing the ratio of recycle to fresh feed the required viscosity can always be achieved; even in the case of only water fed to the inlet.

7.1 CHALLENGES

Maintaining sufficient feed viscosity will be a requirement of effective operation. We have tested a mixture of grass with potato simulant as feed material for the current equipment. This does allow observed temperatures greater than using simulant alone. We also believe that other biomass, such as saw dust and paper, could be used to increase the viscosity of the feed mixture.

For cases where people have diarrhea, where urine is not separated or when water is added by rain or other means, this technology will require a modified design. As part of a Phase 2 project, we will propose equipment modifications that take full advantage of generated heat to evaporate and recover water in fecal solids; which, in turn, will allow some of the processed solids to be recycled into the feed stream for viscosity control. By balancing the ratio of recycle to fresh feed, the required viscosity can always be achieved. Even with all water feed and high recycle, viscous heating can be sufficient to vaporize the water for sanitized condensation.

Another challenge is to reduce the energy consumption to rotate the inner core. This will be addressed by considering different geometries or construction materials focusing on heat transfer properties and rotational momentum. Our goal is to find the optimized power requirement to operate the equipment.

A significant challenge is to separate debris such as gravel, bottle caps, coins, cloth and other trash that would block or bind the mechanics. This will require screening or segregation. As such,

this technology, while highly effective for controlled feed streams, will require integration with associated technologies in practical settings. However, its use within an integrated system will result in sanitation of fecal waste for safe handling, subsequent processing or transportation. Sanitized solids could potentially be used as nutrient material in agricultural applications. It may also retain some energy for thermal or bioconversion processes. Evaporated water recovered from the process would be sanitized for safe use in non-potable applications, but would require further treatment to be consumable.

7.2 FECAL SLUDGE BUSINESS

Fecal sludge is produced from different sources which includes septic tank, activated sludge system, vault latrine and bucket latrine. The treatment of sludge is generally dictated by the characteristics of the sludge. There are several ways for treating fecal sludge, methods such as stabilization, thickening, dewatering, drying and incineration are being currently used to handle fecal sludge. Some of these methods have potential for creating a business and demand for fecal sludge. Although it might seem that the business of fecal sludge be not a profitable one, but considering prudent processing steps, the business is likely to be a cost-effective one.

First of all, in the poorest socio-economic groups, the treated fecal sludge from the reinvented toilets will reduce the possibility of spreading the diseases leading to cost reduction in the budget of medical and health sectors for both family and the government level. The revenue earned by government by saving this cost would easily help increase the ability to expend more money for the employment and development in other sectors in poor communities.

Secondly, biogas production, electricity generation or soil amendments whichever, process is chosen for making business; they could be a viable in overall consideration. For example, if fecal sludge is considered to produce biogas which could be used instead of traditional natural gas for cooking, the profit will count in no supply of natural gas to kitchen purpose by the government.

That means every individual family will not need to pay for the gas to the government and the government does not need to supply gas to the houses in the locality. A large portion of natural gas could be saved in this way. The natural gas thus saved could be used to increase the production of fertilizer. Thus the fecal sludge business does not need to compete to existing fertilizer market at all. Furthermore, more production of fertilizer will increase the revenue of the government. Again the money saved in this way could be used to upgrade the life style of poor community. Also increase in fertilize production will reduce the retail price of fertilizer, which will benefit for the farmers. In addition, fecal matter has significant value as both a fertilizer and sources of energy. Fecal sludge containing organic carbon can be used to condition soil after stabilization. Fecal sludge contains nitrogen and phosphorous, hence, it can be used as an alternative to commercial fertilizers. Its collection and use could be a viable business model around the world by process like composting. Composting is an aerobic bacterial decomposition process that converts fecal sludge into stable organic waste. The end product can be used as soil conditioner. Similarly, anaerobic digestion can be used to produce biogas.

Thirdly, with a minimal training, the cleaning personnel (sweeper) previously involved in fecal sludge disposal can be converted into an efficient technician for the upcoming biogas plant. Since a good number of manual workers are involved in packing fertilizer and earning of these workers would be higher than that of the cleaning personnel, the rest of the workers in this sludge disposal profession could be employed in growing fertilizer factories without any training for packing purpose. This employment will improve their earning and living standards. One approach for creating a profitable business from fecal sludge would be to run a mobile treatment facility. Our concept involves installing a sludge treatment reactor on a truck. The reactor would process the sludge using viscous heating and pressure to produce a sterile and stable end product. The mobile treatment facility can connect several communities. The profit can be generated by either selling the end product back to the communities as an alternative fertilizer and soil conditioner either free

or charging a processing fee. This concept does not require heavy infrastructure or investment and can be easily integrated to the current facilities.

The Gates Foundation expects technology to cost less than 5 cents/person/day, and intends to drive a technology to a penny/person /day. The clear focus is to convince others of the value of the waste, set up appropriate business models for its use, link technologies for multiple overall solutions, establish partnerships for both technologies and business ventures.

REFERENCES

1. Beer, F., Johnston, E. 1990 Vector Mechanics for Engineers, 2nd SI Metric Ed. Chapter 9. McGraw-Hill Book Co.Singapore.
2. Bethony, J., S. Brooker, M. Albonico, S. M. Geiger, A. Loukas, D. Diemert, R. J. Hotez 2006 Soil-transmitted helminth infections: ascariasis, trichuriasis, and hookworm. *The Lancet*. **367**(9521), 1521-1532.
3. Bundy, D.A., D.E. Thompson, M.H. Golden, E.S. Cooper, R.M. Anderson, P.S. Harland 1985 Population distribution of *Trichuris trichiura* in a community of Jamaican children *Trans R Soc Trop Med Hyg.***79**(20), 232-7.
4. Burg,J. P, T.V. Gerya 2005 The role of viscous heating in Barrovian metamorphism of collisional orogens: thermomechanical models and application to the Lepontine Dome in the Central Alps. *Journal of Metamorphic Geology*. **23**(2), 75-95
5. Collins N.W. 1983 A Finite Difference Analysis for Laminar Heat Transferr of Non-Newtonian Fluids in Circular Tubes. *Numerical methods in thermal problems*. 540-550.
6. COMSOL MULTIPHYSICS 2011 *COMSOL Multiphysics User's Guide*. Stockhlom, Sweden: Version 4.2a.
7. Costa, A., G. Macedonio 2005 Viscous heating effects in fluids with temperature-dependent viscosity: triggering of secondary flows. *Journal of Fluid Mechanics* .**540**, 21-

8. Cross, John H. 1996 Enteric Nematodes of Humans. In: Medical Microbiology, 4th Edition, ed. Samuel Baron .Chapter 90. Texas, USA: University of Texas Medical Branch at Galveston. Available from: http://www.ncbi.nlm.nih.gov/books/NBK8261/?redirect-on-error=__HOME__
9. Dinh, S.M., Armstrong, R.C. 1982 Non-Iso thermal Channel Flow of Non-Newtonian Fluids with Viscous Heating. *AIChE Journal*. **28**(2),294-301.
10. Doucleff, Michael 2012 August 10 Why is the world's largest foundation buying fake poop. Retrieved from <http://www.npr.org/blogs/health/2012/08/08/158447235/why-is-the-worlds-largest-foundation-buying-fake-poop#more>.
11. Ellis, H.M., Ring, S.G., Whittam, M.A. 1989 A Comparison of the Viscous Behaviour of Wheat and Maize Starch Pastes. *Journal of Cereal Science* .**10**, 33-44.
12. ___Engineering Tool box (2013) www.engineeringtoolbox.com/specific-heat-capacity-food-d_295.html. (accesses: 15 June 2013).
13. Gifford, W. A. 1997 The use of three dimensional computational fluid dynamics in design of extrusion dies. *Journal of Reinforced Plastics and Composites*. **16**, 661-674.
14. Gresho, P. M. & Sani, R. L. 1998 *Incompressible flow and the finite element method, Volume 2, Isothermal Laminar flow*. Wiley, New York.
15. Heitmann, D., A. Munchen 1995 Determination of the Intrinsic Viscosity of Native Potato Starch Solutions. *Starch*. **47** (11), 426-429.
16. Hooman, K., A. Ejlali 2010 Effects of viscous heating, fluid property variation, velocity slip, and temperature jump on convection through parallel plate and circular microchannels. *International Communications in Heat and Mass Transfer*. **37**(1), 34-38.

17. Lawal, A., D.M. Kalyon 1997 Viscous heating in nonisothermal die flows of viscoplastic fluids with wall slip. *Chemical Engineering Science*. **52**(8), 1323-1337.
18. Murray., G., 1997 Handbook of Materials Selection for Engineering Applications.Chapter 7. Marcel Dekker Inc. New York.
19. Nokes, C., S.M. Grantham-McGregor, A.W. Sawyer, E.S. Cooper, B.A. Robinson, D.A. Bundy 1962 Moderate to heavy infections of *Trichuris trichiura* affect cognitive function in Jamaican school children. *Parasitology*. **104**(3) 539-547.
20. Singh, N., N. Isono, S. Srichuwong,T. Noda, K. Nishinari. 2008 Structural, thermal and viscoelastic properties of potato starches. *Food Hydrocolloids*. **22**(6), 979-988.
21. Smith, H.M., R. DeKaminsky, S. Niwas, R. Soto & P. Jolly 2001 Prevalence and intensity of infections of *Ascaris lumbricoides* and *Trichuris trichiura* and associated socio-deographic variables in four rural Honduran communities. *Mem Inst Oswaldo Cruz, Rio de Janeiro*. **96**(3), 303-314.
22. Takahashi, T., M. Goto, T. Sakata. 2004 Viscoelastic properties of the small intestinal and caecal contents of the chicken. *British Journal of Nutrition*. **91**(6), 867-872.
23. Takahashi, T., T. Sakata. 2002 Large Particles Increase Viscosity and Yield Stress of Pig Cecal Contents without Changing Basic Viscoelastic Properties. *The American Society of Nutritional Science*. **132**(5), 1026-1030.
24. ____, *Trichuris Trichiura (Whipworm)* 2012 Capitola, United States, Capitola: Timely Data Resources, Inc, <http://search.proquest.com/docview/924749458?accountid=4117>.

25. Santo Domingo, S., J. W., J. Lu, O.C. Shanks, R. Lamendella, C.A. Kelty, and D.B. Oerther. 2007 Development of Host-Specific Metagenomic Markers for Microbial Source Tracking Using A Novel Metagenomic Approach. *Disinfection*. **16**,646-661.
26. Schertenleib, R., Forster, D., Belevi, H. 2004 An Integrated Approach to Environmental Sanitation and Urban Agriculture. *Acta Hort. (ISHS)* **643**,223-226.
27. Sunden, B. 1992 Viscous Heating in Forced Convective Heat-Transfer across a Circular-Cylinder at Low Reynolds-Number. *International Journal for Numerical Methods in Engineering*. **35**(4), 729-736.
28. Trönnberg, L., D. Hawksworth, A. Hanses, C. Archer, T. A. Stenstrom. 2010 Household-based prevalence of helminths and parasitic protozoa in rural KwaZulu-Natal, South Africa, assessed from faecal vault sampling. *Transactions of the Royal Society of Tropical Medicine and Hygiene*. **104**(10), 646-652.
29. Vlachopoulos, J. 2003 The Role of Rheology in Polymer Extrusion. *New Technologies for Extrusion*. Milan, Italy.
30. Woolley, Stuart. Personal Communication to Gary L. Foutch. November 02. 2012.
31. ____, Sanitation Network Science & Technology (2012) <http://scitech.sanitationnetwork.org/>. (accessed: 03 June 2012).
32. ____, World Health Organization. 2012 Water, sanitation and hygiene links to health webpage http://www.who.int/water_sanitation_health/publications/facts2004/en/. (accessed: 12 Sep 2012).

33. Yavuz, T., O. Erol, M. Kaya. 2011 Heat transfer characteristics of laminar annular duct flow with viscous dissipation. *Proceedings of the Institution of Mechanical Engineers Part C- Journal of Mechanical Engineering Scienc.* **225**(C7), 1681-1692.
34. Yesilata, B. 2002 Viscous heating effects in viscoelastic flow between rotating parallel-disks. *Turkish journal of engineering & environmental sciences* **26**(6), 503-511.

APPENDICES

APPENDIX A

INSTALLATION OF THE SHEAR REACTOR



Figure 43. Installation of the Cone

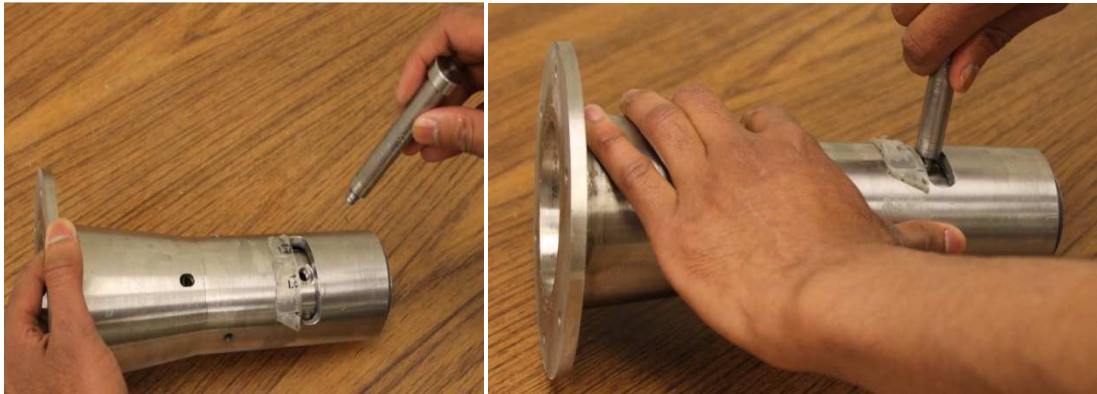


Figure 44. Installation of the Shell



Figure 45. Installation of the Cone and Shell



Figure 46. Installation of Tapered Bottom Bearing



Figure 47. Installation of Nut and Set Screw



Figure 48. Installation of Rectangular Joint



Figure 49. Installation of Lovejoy Coupling

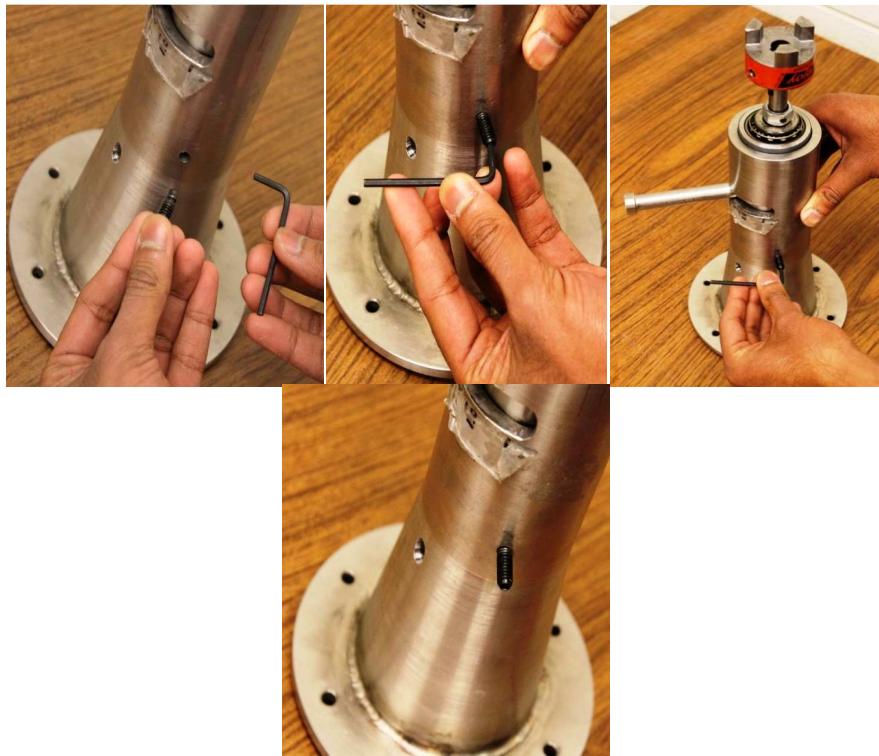


Figure 50. Installation of Shivel Screw to Spacing Controller Cylinder



Figure 51. Installation of Reactor Assembly to the Motor

The feed chamber is then installed on the mountain plate and the inlet piston is installed.

APPENDIX B

OPERATING MANUAL OF THE SHEAR REACTOR

Precheck

1. Make sure the general workspace is clean and tidy.
2. Examine all cords and electrical connections for frays or exposed wiring.
3. Check mobility of the motor for torque measurement.
4. Ensure all mechanical moving parts are unobstructed.
5. Ensure air line, inverter and Remo (torque meter) connections are clear.
6. Do not operate the machine when you are hungry, tired or emotional. You might ruin the experiment as well as the machine.

Emergency Shutdown Procedure

1. In the case of any grinding or other unexpected sound turn the unit power off immediately by unplugging the unit.
2. For any indications of overheating; such as temperature readout, smoking, glow, etc.; turn the power off immediately by unplugging the unit.
3. Notify others of potential hazards.
4. DO NOT start the unit again until expected by faculty/staff.
5. Push emergency stop button with any noise or erratic sounds. Consult with manufacturer or authorized service person.



Figure 52. Emergency Shutdown Button

Normal Operating Procedure

1. Prepare formulation of mass to be evaluated following separate procedure
2. Place the mass into the feed cell.
3. Move the plunger assembly past the feed port.
4. Adjust the spacing of the extruder for the specific sampling test.
5. Start the motor and observed whether all appears to be operating correctly.
6. Start the plunger and allow the feed mass to enter the extruder space.
7. Observe and record temperatures.
8. Observe and collect mass exiting the extruder zone.
9. Record torque
10. Record air pressure
11. Record Extruder spacing
12. Record temperature of outlet product

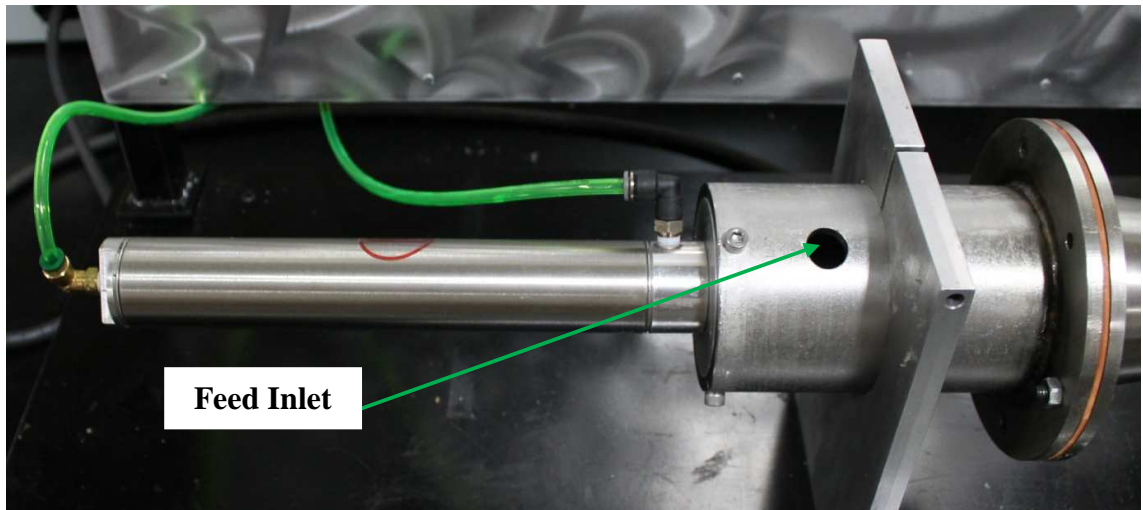


Figure 53. Feed Inlet

Preparation of Mass (Sample)

1. Boil potatoes according to need until get thawed.
2. Wait at least 20 minutes to cool down the potatoes to near ambient temperature.
3. For faster cooling sink the potatoes in cold tap water.
4. Remove all the skins from the boiled potatoes by hand. (wearing gloves will be practice of good science)
5. Put all potatoes in appropriate blender/grinder so they get mashed.
6. For each experiment take mashed potatoes of 100 to 120 grams approximately.

Evaluation of mass

1. Weigh a sample
2. Place in drying oven
3. After 24 hours reweigh and determine mass loss
4. Record all the masses

Starting the Motor

1. Plug the unit into the appropriate 230 VAC power source and rotate the plug after inserting into the socket.
2. Before starting the inverter check all the electric connection are properly and tightly connected. (use only one hand to check the connections)
3. This machine is operable less than 100,000 rms Symmetrical Amperes, 240 or 480V maximum.
4. Push “Run” key to inverter run.



RUN Button

Figure 54. WJ 200Series 3 Phase Inverter

5. The inverter can vary speed of the motor according to experimental specification
6. Using Up and Down arrow key, the motor speed can be changed.
7. STOP/RESET key can be used to stop the inverter.
8. Do not change any of the function codes.

9. Do not press the Escape (ESC) key. Pressing the Escape key puts the controller into programming mode. The unit power will have to be cycled off to reset the unit into operating mode.
10. Do not keep hand or do not touch the coupling joint when the rotor starts rotating if there is no cover there. If there is a cover do not remove the cover.
11. If the emergency stop is pressed, the motor will need to be reset by returning the emergency stop button to the out position and then pressing the stop/reset button on the control unit.

Air Feeding

1. Make sure the air feed line is clean and obstacle free. It might have some smashed potato which might block the air flow.
2. Connect the air pipe to the inlet of air regulator which is situated behind the vertical metal board. Open the air inlet valve to allow the air to enter.
3. The air feed pressure will be shown in the pressure gauge. Pressure range will be 0 to 100 psig.
4. Under the pressure gauge there is yellow pressure regulator. Air feed pressure can be controlled by the regulator. Rotate the regulator to achieve desired pressure you need.

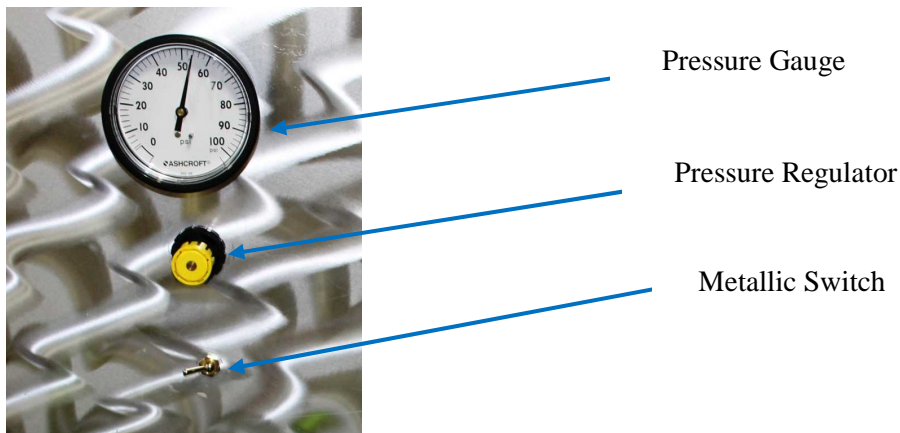


Figure 55. Pressure Gauge, Pressure Regulator and Switch

5. There is a small metallic switch just under the yellow pressure regulator which can control the direction of air flow. Pressing it to the right or left will make the feed piston retract to the loading position. Switching the lever to the middle position will cause the piston to advance toward the test section of the unit and compress the feed stock into the rotor.

Spacing Control

1. The rotating shaft inside the housing will be rotating according to desired spacing fixed by user. The metallic handle can be moved back and forth to have desired spacing. Use the calibration to get desired spacing.

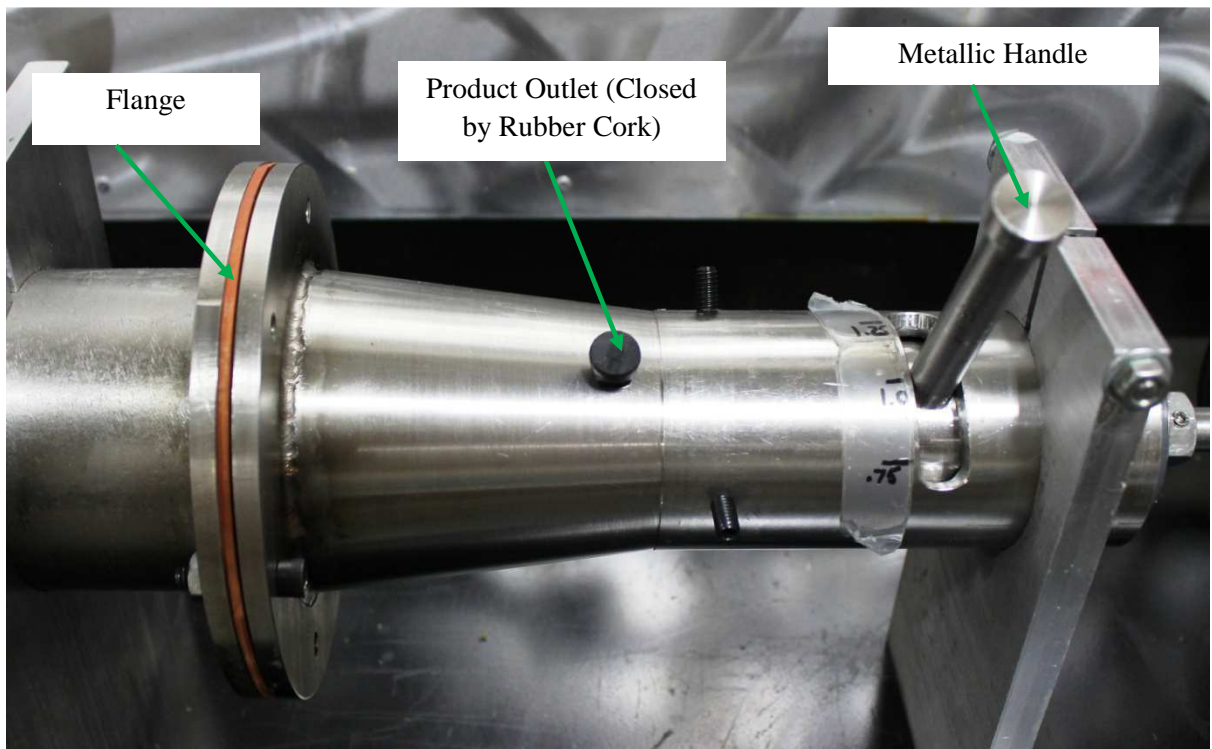


Figure 56. Flange, Product Outlet and Metallic Handle

2. The spacing between the housing and rotating shaft will be increased if the metal handle is pushed forward to the vertical metal wall (Anticlockwise direction if you look at from the side of air cylinder inlet) and vice versa
3. Do not put your finger in the inlet while the plunger is working.

4. Do not put your hand or fingers in the outlet of the machine. The emerging product is hot enough (200°C) to cause burns. If mistakenly touched by skin wash skin with continuous flow water at least 15 minutes.

Cleaning up the Extruder

1. Allow the reactor to be cold near to room temperature.
2. Switch off the inverter and unplug it.
3. Unplug the air inlet pipe.
4. Remove three screws and separate air piston.
5. Remove screws from reactor parts also.

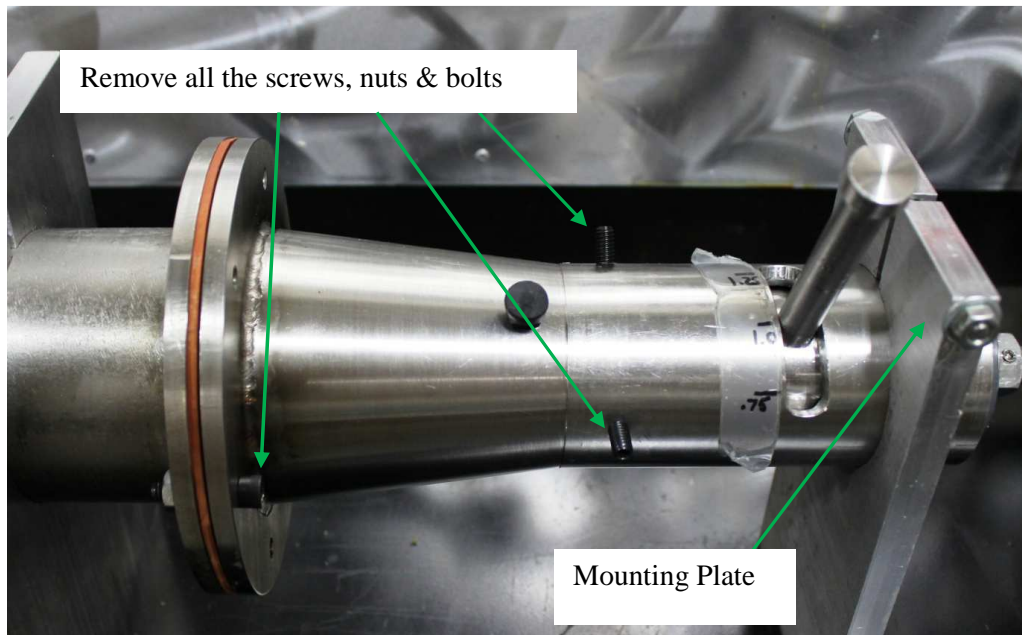


Figure 57. Nuts & Bolts of the Reactor

1. Under the horizontal base of the equipment, there are four bolts to keep rigid the mounting plates. Unscrew the bolts.
2. Remove all the bolts and nuts from the flange.
3. Thoroughly wash the feed point, reactor and flanges with warm water and ensure the unit is properly cleaned.

4. If some sticky material is found, that is not possible to remove with one washing, keep the reactor wet with warm water for 10 minutes and wash again thoroughly.
5. Make all the parts dry.
6. Build the unit again and get ready for next experiment.

APPENDIX C

MODEL DEVELOPMENT

We have other experimental results for variable settings. Those are presented from table 14 to table 26 and from figure 47 to figure 58.

Table 14. Outlet Temperature for Different Hold up Time at 0.75mm Spacing, 1210 RPM and 100 psig Feed Pressure

Feed	Feed Pressure	RPM	Spacing	Hold up Time	Outlet Temperature
	psig		mm	seconds	°C
Red Potato	100	1210	0.75	0	34.5
				60	50
				120	62
				180	72
				240	96
				300	125

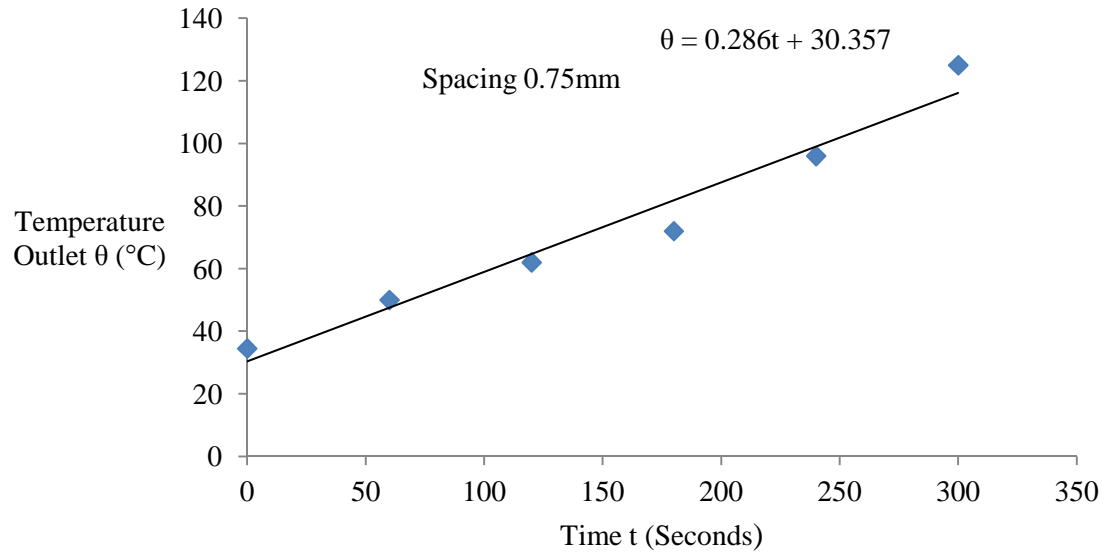


Figure 58. Outlet Temperature for Different Hold up Time at 0.75mm Spacing, 1210 RPM and 100 psig feed Pressure (Corresponding Plot of Table 14)

Table 15. Outlet Temperature for Different Hold up Time at 1mm Spacing, 1210 RPM and 100 psig Feed Pressure

Feed	Feed Pressure	RPM	Spacing	Hold up Time	Outlet Temperature
	psig		mm	seconds	°C
Red Potato	100	1210	1.00	0	42
				60	55
				120	62
				180	70
				215	130

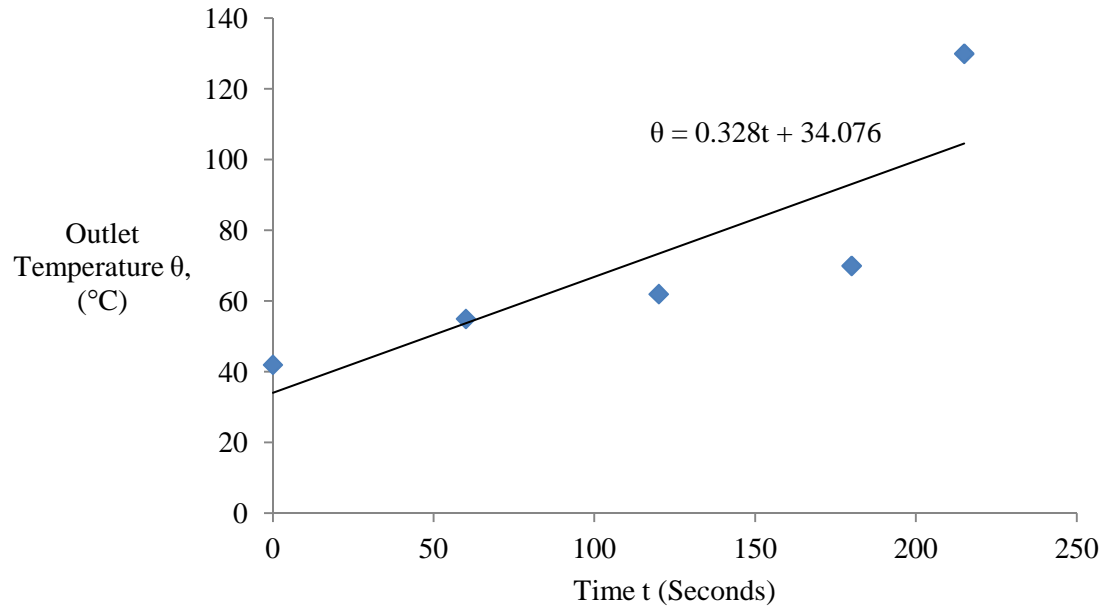


Figure 59. Outlet Temperature for Different Hold up Time at 1mm Spacing, 1210 RPM and 100 psig Feed Pressure (Corresponding Plot of Table 15)

Table 16. Outlet Temperature for Different Hold up Time at 1.25 mm Spacing, 1210 RPM and 100 psig Feed Pressure

Feed	Feed Pressure	RPM	Spacing	Hold up Time	Outlet Temperature
	psig		mm	seconds	$^{\circ}\text{C}$
Red Potato	100	1210	1.25	0	20.3
				60	39
				120	43
				180	50
				240	61
				260	90

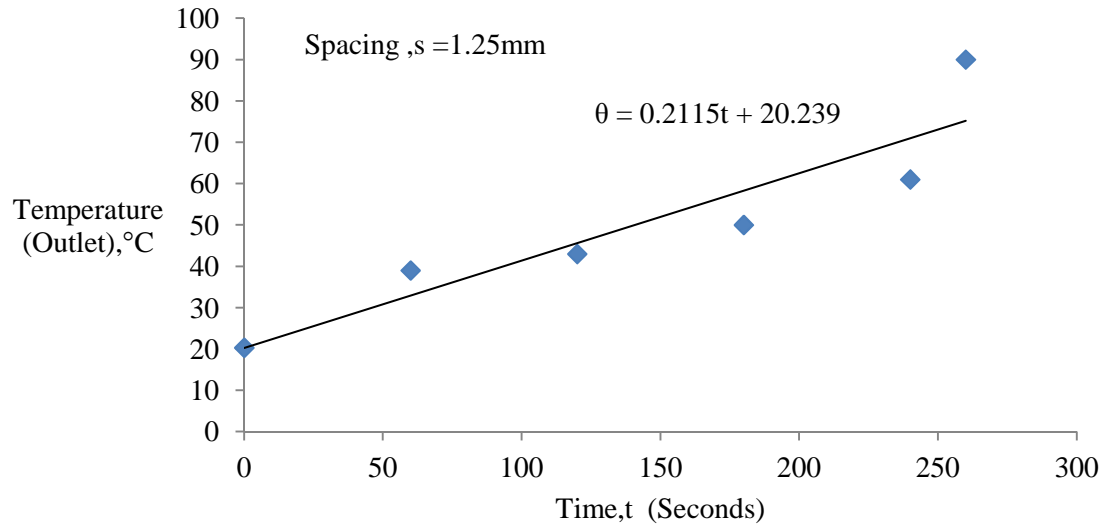


Figure 60. Outlet Temperature for Different Hold up Time at 1.25 mm Spacing, 1210 RPM and 100 psig Feed Pressure (Corresponding Plot of Table 16)

Table 17. Outlet Temperature for Different Hold up Time at 0.75 mm Spacing, 1800 RPM and 100 psig Feed Pressure

Feed	Feed Pressure	RPM	Spacing	Hold up Time	Outlet Temperature
	psig		mm	seconds	°C
Red Potato	100	1800	0.75	0	34
				60	64
				120	74
				180	86
				240	162
				260	190

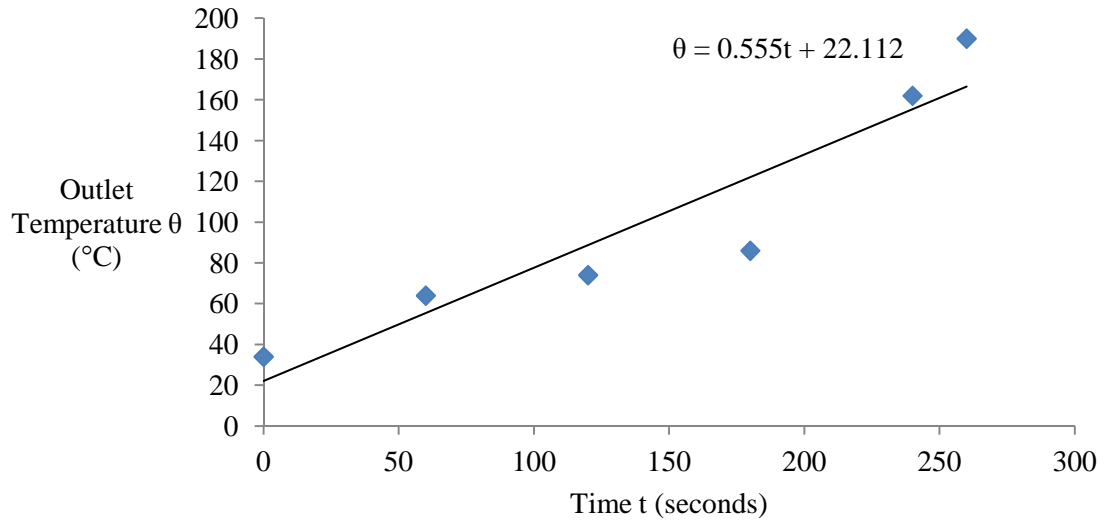


Figure 61. Outlet Temperature for Different Hold up Time at 0.75 mm Spacing, 1800 RPM and 100 psig Feed Pressure (Corresponding Plot of Table 17)

Table 18. Outlet Temperature for Different Hold up Time at 0.75 mm Spacing, 1505 RPM and 100 psig Feed Pressure

Feed	Feed Pressure	RPM	Spacing	Hold up Time	Outlet Temperature
	psig		mm	seconds	$^{\circ}\text{C}$
Red Potato	100	1505	0.75	0	19
				60	45
				120	62
				180	104
				240	110

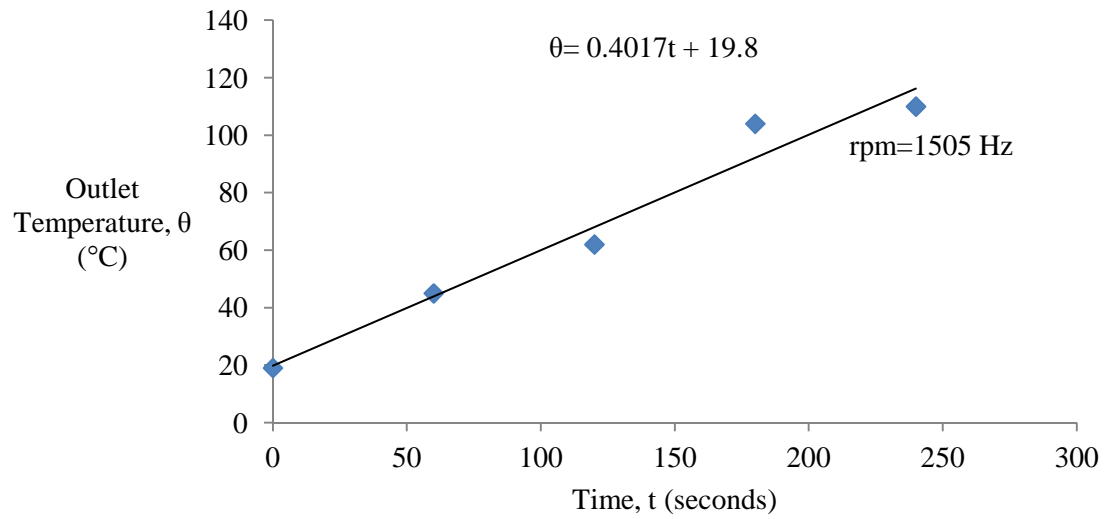


Figure 62. Outlet Temperature for Different Hold up Time at 0.75 mm Spacing, 1505 RPM and 100 psig Feed Pressure (Corresponding Plot of Table 18)

Table 19. Outlet Temperature for Different Hold up Time at 0.75 mm Spacing, 1210 RPM and 100 psig Feed Pressure

Feed	Feed Pressure	RPM	Spacing	Hold up Time	Outlet Temperature
	psig		mm	seconds	°C
Red Potato	100	1210	0.75	0	34.5
				60	50
				120	62
				180	72
				240	96
				300	125

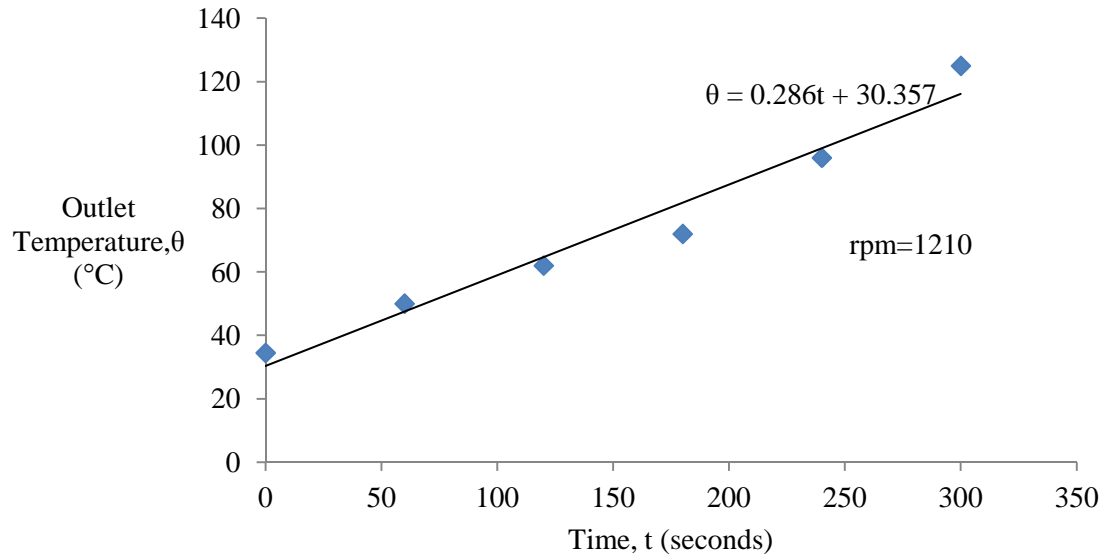


Figure 63. Outlet Temperature for Different Hold up Time at 0.75 mm Spacing, 1210 RPM and 100 psig Feed Pressure (Corresponding Plot of Table 19)

Table 20. Outlet Temperature for Different Hold up Time at 0.75 mm Spacing, 912 RPM and 100 psig Feed Pressure

Feed	Feed Pressure	RPM	Spacing	Hold up Time	Outlet Temperature
	psig		mm	seconds	°C
Red Potato	100	912	0.75	0	22
				60	40
				120	49
				180	55
				240	127

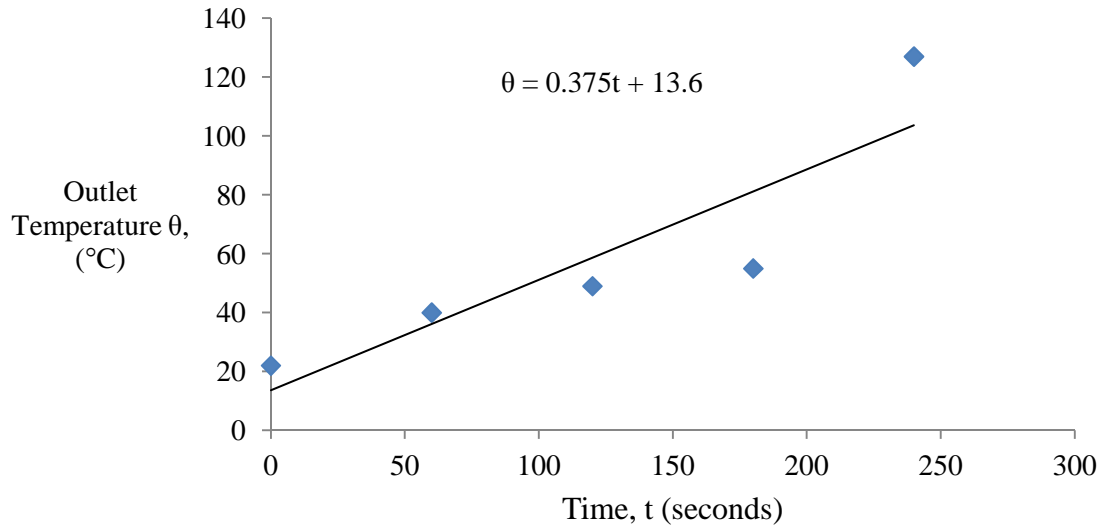


Figure 64. Outlet Temperature for Different Hold up Time at 0.75 mm Spacing, 912 RPM and 100 psig Feed Pressure (Corresponding Plot of Table 20)

Table 21. Outlet Temperature for Different RPM at 0.75 mm Spacing, 180 seconds Holdup Time and 100 psig Feed Pressure

Feed	Feed Pressure	Holdup Time	Spacing	RPM	Outlet Temperature
	psig	Seconds	mm		°C
Red Potato	100	180	0.75	912	55
				1210	72
				1505	104

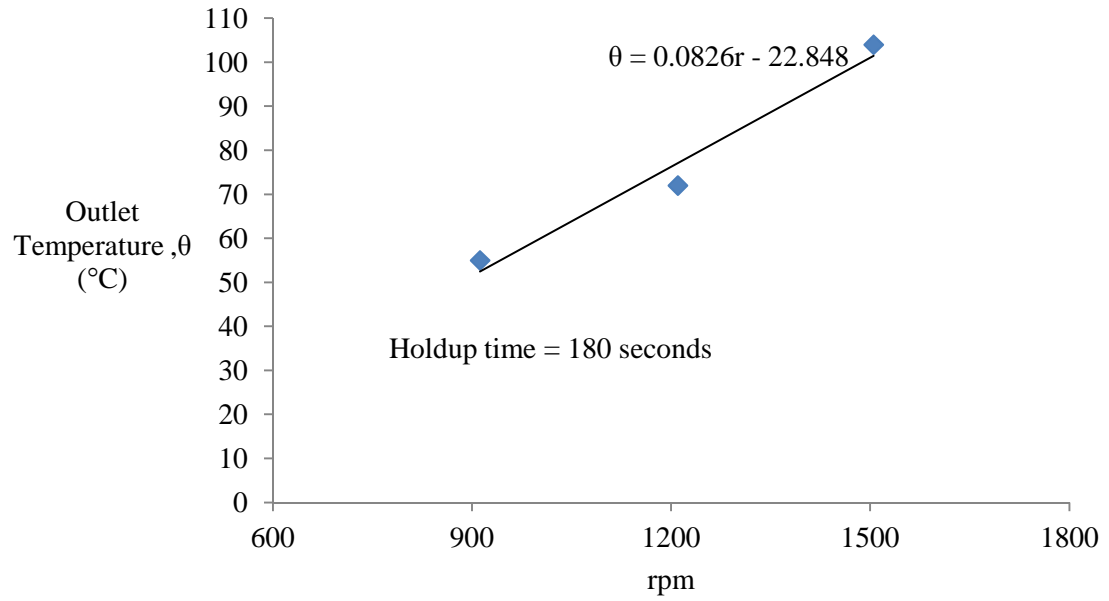


Figure 65. Outlet Temperature for Different RPM at 0.75 mm Spacing, 180 seconds Holdup Time and 100 psig Feed Pressure (Corresponding Plot of Table 21)

Table 22. Outlet Temperature for Different RPM at 0.75 mm Spacing, 120 seconds Holdup Time and 100 psig Feed Pressure

Feed	Feed Pressure	Holdup Time	Spacing	RPM	Outlet Temperature
	psig	Seconds	mm		°C
Red Potato	100	120	0.75	912	49
				1210	62
				1505	120
				1800	134

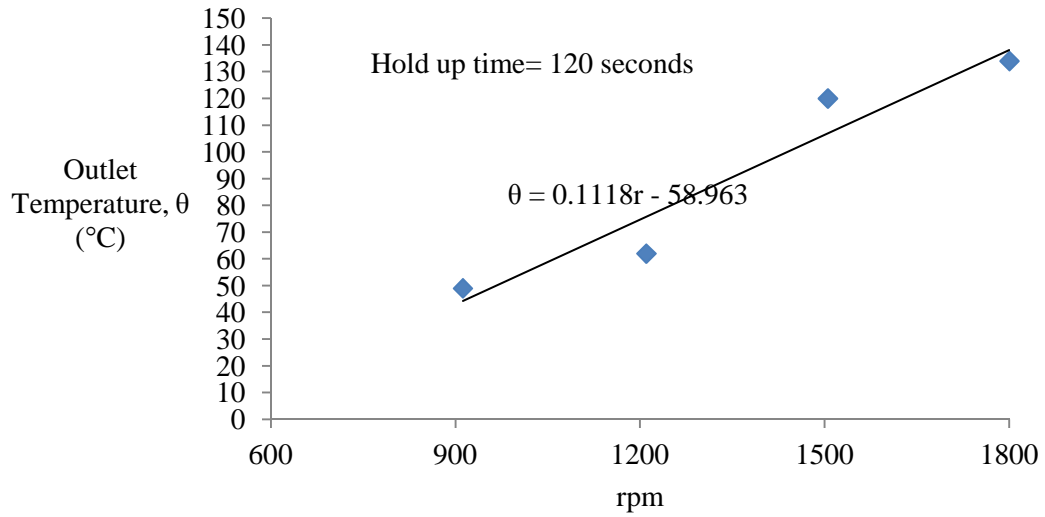


Figure 66. Outlet Temperature for Different RPM at 0.75 mm Spacing, 120 seconds Holdup Time and 100 psig Feed Pressure (Corresponding Plot of Table 22)

Table 23. Outlet Temperature for Different RPM at 0.75 mm Spacing, 60 seconds Holdup Time and 100 psig Feed Pressure

Feed	Feed Pressure	Holdup Time	Spacing	RPM	Outlet Temperature
	psig	Seconds	mm		°C
Red Potato	100	60	0.75	761	59
				912	40
				1210	50
				1505	45
				1800	64

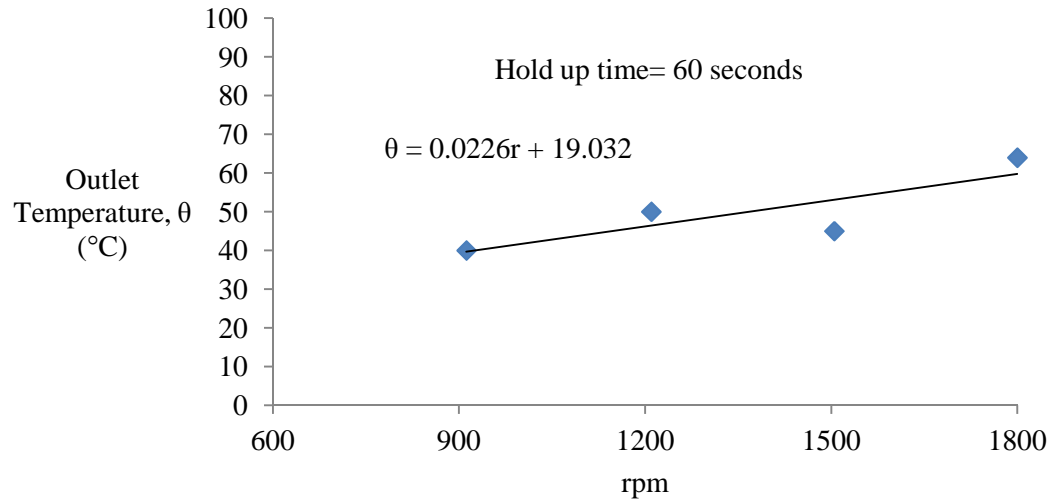


Figure 67. Outlet Temperature for Different RPM at 0.75 mm Spacing, 60 seconds Holdup Time and 100 psig Feed Pressure (Corresponding Plot of Table 23)

Table 24. Outlet Temperature for Different Spacing at 180 seconds Holdup Time, 1210 RPM and 100 psig Feed Pressure

Feed	Feed Pressure	RPM	Hold up Time	Spacing	Outlet Temperature
	psig		seconds	mm	°C
Red Potato	100	1210	180	0.75	72
				1.00	70
				1.25	50

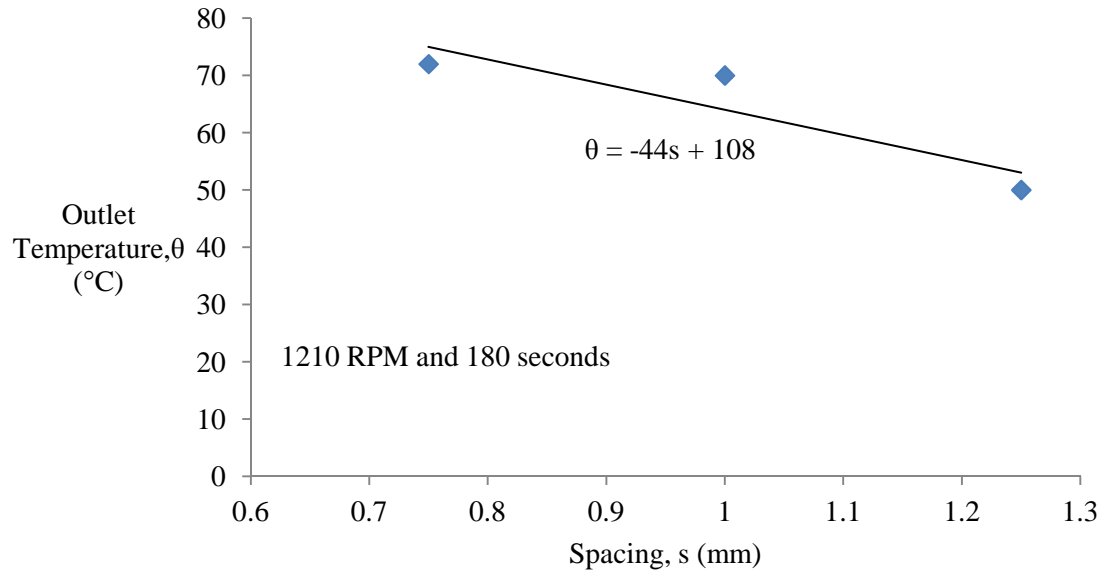


Figure 68. Outlet Temperature for Different Spacing at 180 seconds Holdup Time, 1210 RPM and 100 psig Feed Pressure (Corresponding Plot of Table 24)

Table 25. Outlet Temperature for Different Spacing at 120 seconds Holdup Time, 1210 RPM and 100 psig Feed Pressure

Feed	Feed Pressure	RPM	Hold up Time	Spacing	Outlet Temperature
	psig		seconds	mm	°C
Red Potato	100	1210	120	0.75	62
				1.00	62
				1.25	43

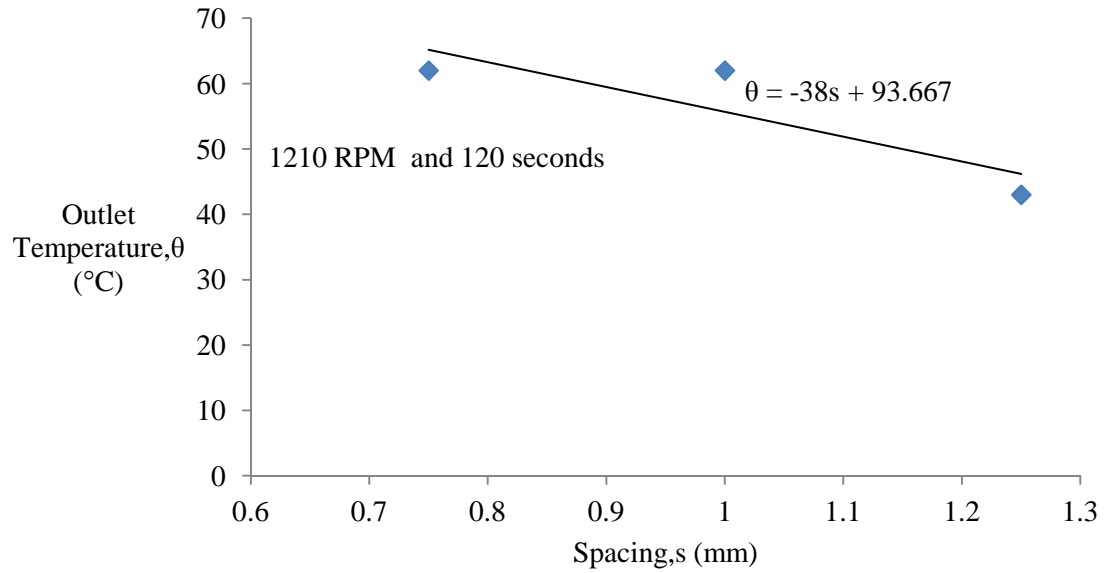


Figure 69. Outlet Temperature for Different Spacing at 120 seconds Holdup Time, 1210 RPM and 100 psig Feed Pressure (Corresponding Plot of Table 25)

Table 26. Outlet Temperature for Different Spacing at 60 seconds Holdup Time, 1210 RPM and 100 psig Feed Pressure

Feed	Feed Pressure	RPM	Hold up Time	Spacing	Outlet Temperature
	psig		seconds	mm	°C
Red Potato	100	1210	60	0.75	50
				1.00	55
				1.25	39

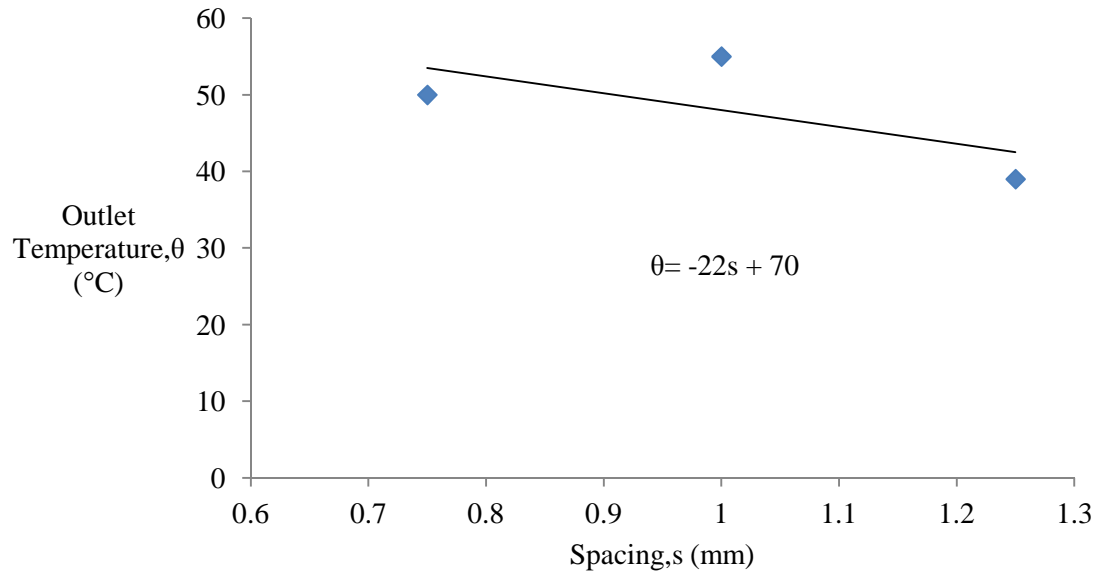


Figure 70. Outlet Temperature for Different Spacing at 60 seconds Holdup Time, 1210 RPM and 100 psig Feed Pressure (Corresponding Plot of Table 26)

As we see, temperature rise due to viscous heating is depending on three variables at constant pressure. Those are rpm, spacing and hold up time. A model could be developed for a constant feed pressure operation.

The governing model equation for a constant feed pressure could be

$\theta = f(r, s, t)$ where

$\theta =$ Outlet temperature ($^{\circ}\text{C}$)

$r =$ rotation per minute (RPM)

$s =$ spacing (mm)

$t =$ Hold up time (seconds)

Now suppose for figure 58, we have an equation of outlet temperature,

$$\theta = -22s + 70 \quad (26)$$

For 60 seconds Holdup Time, 1210 RPM and 100 psig Feed Pressure

Differentiating equation with respect to s we have

$$\frac{\partial \theta}{\partial s} = -22 \quad (\text{Where } t \text{ and } r \text{ are constant at 100 psig feed pressure})$$

Similarly we can obtain different partial values presented from the equations of figure 47 to figure 58. Those differential values could be used to develop the model or correlation for out let temperature θ . Data are present from table 27 to table 30.

Table 27. $\frac{\partial \theta}{\partial t}$ Values with Different RPM at 0.75mm Spacing

s	r	$\frac{\partial \theta}{\partial t}$
mm	RPM	°C/second
0.75	912	0.375
	1210	0.286
	1505	0.4017
	1800	0.555

Table 28. $\frac{\partial \theta}{\partial t}$ Values with Different Spacing at 1210 RPM

r	s	$\frac{\partial \theta}{\partial t}$
RPM	mm	°C/second
1210	0.75	0.286
	1.00	0.328
	1.25	0.2115

Table 29. $\frac{\partial\theta}{\partial r}$ Values with Different Holdup Time at 0.75 mm Spacing

s	t	$\frac{\partial\theta}{\partial r}$
mm	seconds	°C/RPM
0.75	60	0.0226
	120	0.1118
	180	0.0826

Table 30. $\frac{\partial\theta}{\partial s}$ Values with Different Holdup time at 1210 RPM

r	t	$\frac{\partial\theta}{\partial s}$
RPM	seconds	°C/mm
1210	60	-22
	120	-38
	180	-44

APPENDIX D

Table 31. Hz (inverter reading) and Tachometer Reading without Any Load

Hz (Inverter Reading)	RPM (Tachometer Reading)
60	1800
55	1653
50	1505
45	1360
40	1210
35	1061
30	912

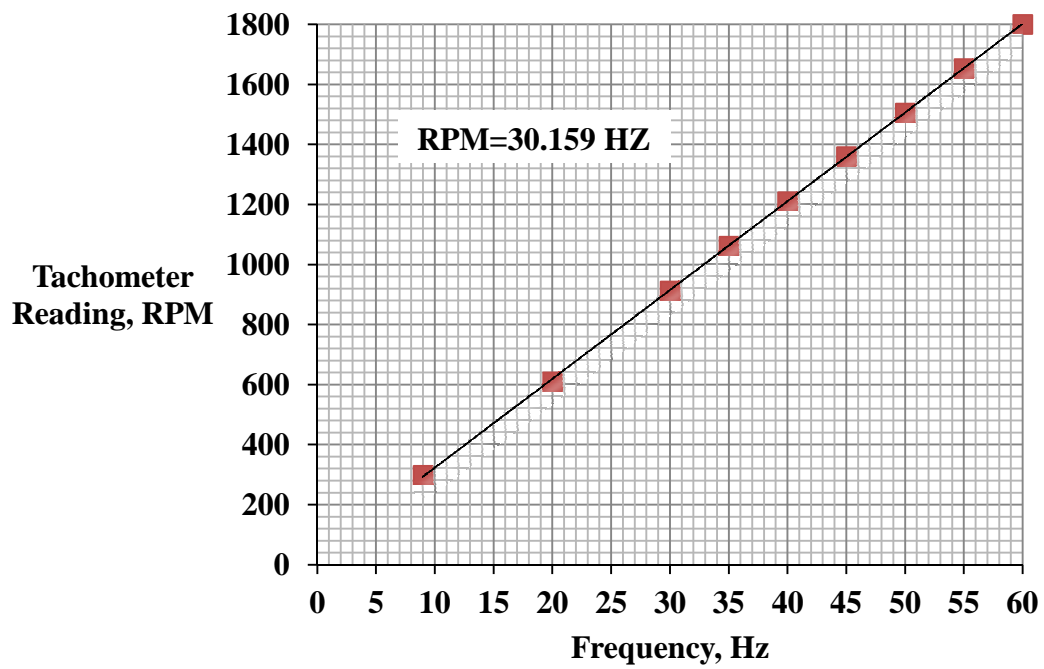




Figure 71. Tachometer Reading (RPM) vs Frequency


APPENDIX E

ROTATING PARTS

Photo of the Rotating Parts	Name	Weight
	Cone	2.746 Kg

			<p>Love Joy Joint</p>	<p>214 gm</p>
			<p>Star Joint Connector</p>	<p>12.7506 gm</p>

			Nut	12.7087 gm
				1.5775 gm

			Black Rubber Seal	1.7926 gm
			Tapered Bottom Bearing	58.5588 gm

VITA

Md. Waliul Islam

Candidate for the Degree of

Master of Science

Thesis: CONCEPT OF VISCOUS HEATING TO REINVENT THE TOILET

Major Field: Chemical Engineering

Biographical:

Education:

Completed the requirements for the Master of Science in Chemical Engineering at Oklahoma State University, Stillwater, Oklahoma in May, 2013.

Completed the requirements for the Bachelor of Science in Chemical Engineering at Bangladesh University of Engineering & Technology, Dhaka, Bangladesh in 2008.

Experience:

Research Assistant January 2012-December 2013
Oklahoma State University Stillwater, Oklahoma

- Assembled, operated and repaired the reactor assembly
- Planned & performed all the experiments and gather data for use
- Proposed new technologies in combination with existing technology
- Assisted editing funding proposal and draft financial & scientific report
- Developed conference presentations and design poster

Teaching Assistant August-December, 2011
Oklahoma State University Stillwater, Oklahoma

- Instructed a class of 25 juniors and supervised students in solving problems
- Encouraged students to overcome course load
- Assessed progress of the group and stimulated for higher goal

Professional Memberships:

Communications Director-GPSGA 2012-2013
Chair-Communications and Publications Committee 2012-2013
Omega Chi Epsilon October 2012-Present
Member-International Society of Automation August 2012-Present
Graduate TA Professional Development Taskforce August-December, 2012